

INFORMATION GEOMETRIC REGULARIZATION OF THE BAROTROPIC EULER EQUATION

RUIJIA CAO* AND FLORIAN SCHÄFER†

Abstract. A key numerical difficulty in compressible fluid dynamics is the formation of shock waves. Shock waves feature jump discontinuities in the velocity and density of the fluid and thus preclude the existence of classical solutions to the compressible Euler equations. Weak “entropy” solutions are commonly defined by viscous regularization, but even small amounts of viscosity can substantially change the long-term behavior of the solution. In this work, we propose the first inviscid regularization of the multidimensional Euler equation based on ideas from semidefinite programming, information geometry, geometric hydrodynamics, and nonlinear elasticity. From a Lagrangian perspective, shock formation in entropy solutions amounts to inelastic collisions of fluid particles. Their trajectories are akin to that of projected gradient descent on a feasible set of non-intersecting paths. We regularize these trajectories by replacing them with solution paths of interior point methods based on log determinantal barrier functions. These paths are geodesic curves with respect to the information geometry induced by the barrier function. Thus, our regularization amounts to replacing the Euclidean geometry of phase space with a suitable information geometry. We extend this idea to infinite families of paths by viewing Euler’s equations as a dynamical system on a diffeomorphism manifold. Our regularization embeds this manifold into an information geometric ambient space, equipping it with a geodesically complete geometry. Expressing the resulting Lagrangian equations in Eulerian form, we derive a regularized Euler equation in conservation form. Numerical experiments on one and two-dimensional problems show its promise as a numerical tool. While we focus on the barotropic Euler equations for concreteness and simplicity of exposition, our regularization easily extends to more general Euler and Navier-Stokes-type equations.

Key words. Compressible flow, shock waves, interior point methods, information geometry, inviscid regularization, geometric hydrodynamics, nonlinear elasticity

MSC codes. 35L65, 76L05, 65M25, 76J20, 58B20

1. Introduction.

1.1. The problem.

The barotropic Euler equation describes an inviscid and barotropic gas

$$(1.1) \quad \partial_t \begin{pmatrix} \rho \mathbf{u} \\ \rho \end{pmatrix} + \overset{\rightarrow}{\text{div}} \begin{pmatrix} \rho \mathbf{u} \otimes \mathbf{u} + P(\rho) \mathbf{I} \\ \rho \mathbf{u} \end{pmatrix} = \begin{pmatrix} \mathbf{f} \\ 0 \end{pmatrix}.$$

Here, $\overset{\rightarrow}{\text{div}}$ denotes the row-wise divergence, $\mathbf{u}(\mathbf{x}, t)$ denotes the velocity of a gas particle passing through a point \mathbf{x} at time t and $\rho(\mathbf{x}, t)$ denotes the gas density in \mathbf{x} at t . Thus, $\boldsymbol{\mu}(\mathbf{x}, t) = \rho(\mathbf{x}, t)\mathbf{u}(\mathbf{x}, t)$ denotes the momentum density in \mathbf{x} at time t . The pressure P depends only on the density and \mathbf{f} denotes external forces acting on the gas.

Shock formation in compressible flows. The steepening of wavefronts is characteristic of compressible flows. It arises from faster upstream particles catching up to slower downstream ones, steepening the slope of \mathbf{u} and forming singular shocks. Shock formation was proved for a wide range of flows [64, 23, 21, 24, 22].

Vanishing viscosity solutions and entropy conditions. Shock waves preclude long-time existence of classical solutions to (1.1). The canonical solution concept are limits of Navier Stokes solutions with vanishing viscosity or refinements thereof [39](see Figure 1). They are also characterized by entropy conditions (see, e.g. [48]).

*Georgia Tech (rcao62@gatech.edu).

†Georgia Tech (fts@gatech.edu).

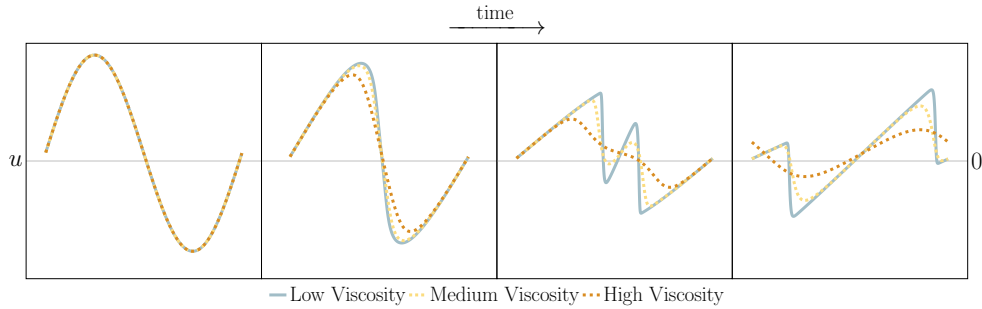


FIG. 1. *Vanishing viscosity solutions.* In the presence of shocks, solutions are defined by vanishing viscosity limits. For finite viscosity, the solution becomes excessively smooth over time.

1.2. Existing approaches.

Localized viscosity. Naive approaches for computing vanishing viscosity solutions require a mesh width proportional to the viscosity parameter, leading to excessive computational cost or energy dissipation. Instead, numerous methods add viscosity *adaptively*, according to shock indicators [66, 57, 27, 32, 52, 10, 38, 17, 29].

Purely numerical remedies emphasize the avoidance of Gibbs oscillations encountered by high-order schemes near shocks using limiters that reduce the approximation order at the shock [65, 59] and (W)ENO-type schemes that select the reconstruction stencil adaptively [50, 41, 63]. The numerical dissipation of low-order methods result in behavior similar to localized viscosity. However, a downside of these methods is the absence of a well-defined PDE. For instance, stencil-switching and slope limiters introduce errors in adjoint-based sensitivities [15, 51].

Inviscid PDE-based regularization. A third line of work aims to develop *inviscid* PDE-based regularizations. First attempts based on [47] failed to capture the correct shock speeds of the Euler equations, making them unsuitable for most applications [14, 13, 12]. [37] proposes inviscid nondispersive regularizations based on [25]. It maintains the correct shock speed but is limited to unidimensional problems.

1.3. This work presents the first multidimensional inviscid Euler regularization.

Interior point methods for Euler. For vanishing P, \mathbf{f} , (1.1) reduces to Burgers' equation, solvable by the method of characteristics. Shocks form when characteristics meet. Viscosity solutions follow solution paths of projected gradient descent under the constraint of non-crossing characteristics. This work modifies characteristics to follow solution paths of interior point methods defined by a barrier ψ [53]. This ensures strict feasibility (avoidance of shocks) while preserving long-term behavior.

Information geometry on diffeomorphism manifolds. To make this idea precise, we use the fact that solution paths of interior point methods are dual geodesics in the information geometry defined by ψ [2, 1]. Collectively, Burgers characteristics describe geodesics on diffeomorphism manifolds [7, 30, 45, 46]. Our regularization replaces them with dual geodesics in the information geometry of ψ . Adding forces of \mathbf{f}, P and returning to a Eulerian description results in the regularized Euler equation

$$(1.2) \quad \begin{cases} \partial_t \begin{pmatrix} \rho \mathbf{u} \\ \rho \end{pmatrix} + \vec{\text{div}} \begin{pmatrix} \rho \mathbf{u} \otimes \mathbf{u} + (P(\rho) + \Sigma) \mathbf{I} \\ \rho \mathbf{u} \end{pmatrix} = \begin{pmatrix} \mathbf{f} \\ 0 \end{pmatrix} \\ \rho^{-1} \Sigma - \alpha \vec{\text{div}}(\rho^{-1} \nabla \Sigma) = \alpha \left(\text{tr}([\mathbf{D}\mathbf{u}])^2 + \text{tr}([\mathbf{D}\mathbf{u}]^2) \right). \end{cases}$$

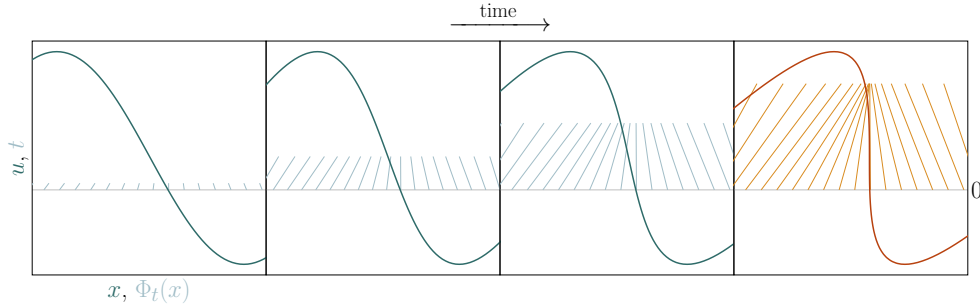


FIG. 2. **Shock formation and characteristics.** The plot overlays the Burgers' characteristics with the velocity profile, at four different time steps. As the characteristics approach each other, the profile steepens. In the rightmost plot, the characteristics cross and the flow develops a shock.

This work focuses on the barotropic Euler equations for concreteness and to simplify the exposition. But one can easily derive extensions to general Euler and Navier-Stokes-type equations by adding the *entropic pressure* Σ to their momentum flux. By choosing $\sqrt{\alpha}$ proportional to the mesh size, the elliptic problem defining Σ in (1.2) can be solved efficiently by a constant number of Jacobi sweeps. One sweep per flux computation often suffices in practice, ensuring negligible computational overhead.

2. Information geometric regularization.

2.1. A Lagrangian view on shock formation.

Model problem: The Burgers equation. For simplicity, we illustrate our approach on the unidimensional case of equation (1.1), with $P, \mathbf{f} \equiv 0$.

$$(2.1) \quad \partial_t \begin{pmatrix} \rho u \\ \rho \end{pmatrix} + \partial_x \begin{pmatrix} \rho u^2 \\ \rho u \end{pmatrix} = \begin{pmatrix} 0 \\ 0 \end{pmatrix} \implies \partial_t \begin{pmatrix} u \\ \rho \end{pmatrix} + \partial_x \begin{pmatrix} u^2/2 \\ \rho u \end{pmatrix} = \begin{pmatrix} 0 \\ 0 \end{pmatrix}.$$

The second equation is often discarded, resulting in $\partial_t u + u \partial_x u = 0$. Smooth solutions of (2.1) describe the inertial movement of noninteracting particles.

Characteristics and shock formation. Burgers' equation is solvable by the method of characteristics [31]. For initial conditions $u(\cdot, 0)$ and a family of curves

$$\Phi_t(x) := x + tu(x, 0), \quad \text{define the solution } u \text{ as } u(\Phi_t(x), t) := u(x, 0).$$

The solution in (x, t) is obtained by tracing the line $\{\Phi_t(y)\}$ passing through x at time t to the initial condition. If y is unique, u satisfies Burgers' equations, since

$$0 = \frac{d}{dt} (u(\Phi_t(x), t)) = \left[\partial_t u + \partial_x \left(\frac{u^2}{2} \right) \right] (\Phi_t(x), t).$$

The $t \mapsto \Phi_t(x)$ are trajectory of particles with initial position x and velocity $u(x, 0)$. Figure 2 shows that Burgers shocks form when these curves cross and $u(x, t)$ can not be traced back to a unique initial condition. In a vanishing viscosity solution, these collisions are fully inelastic and the curves $\Phi_t(x)$ merge as shown in Figure 3.

2.2. Semidefinite programming meets fluid dynamics.

Interior point methods for Euler. Shock formation occurs when characteristics meet. We examine two characteristic curves $t \mapsto (\Phi_t(x_1), \Phi_t(x_2))$ initialized in x_1

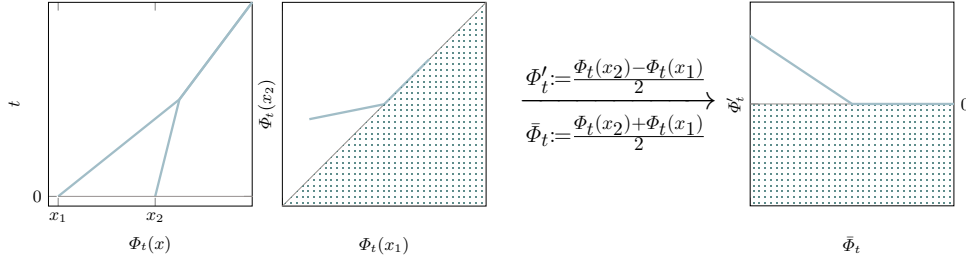


FIG. 3. **Collision of Characteristics.** When Burgers' characteristics cross, they merge and a shock forms. In phase space, this means that the system evolves on the boundary of the feasible set that is accessible without crossing characteristics. In transformed coordinates, it is a half-space.

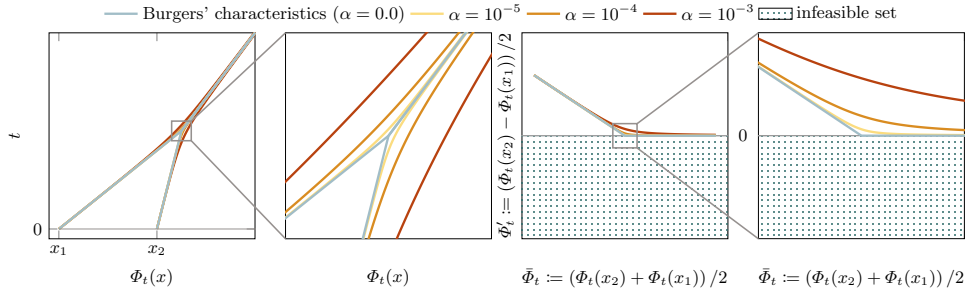


FIG. 4. **Geometric regularization.** Regularizing the $\bar{\Phi}$ - Φ' geometry of a pair of characteristics with the barrier term $\alpha(-\log(\Phi'))$ avoids shock formation while preserving the long-time behavior.

and x_2 . Figure 3 shows the feasible region \mathcal{R} in phase space where shocks do not form. In coordinates $\bar{\Phi}_t = (\Phi_t(x_1) + \Phi_t(x_2))/2$ and $\Phi'_t = (\Phi_t(x_1) - \Phi_t(x_2))/2$, the feasible region \mathcal{R} becomes the positive half space. When reaching the boundary $\partial\mathcal{R}$, a shock forms and the merged characteristics continue on $\partial\mathcal{R}$. This is the solution path of projected gradient ascent on $\max_{\mathbf{v} \in \mathcal{R}} \langle \mathbf{u}_{t=0}(x_1, x_2), \mathbf{v} \rangle$ [18]. In contrast to projection-based approaches, interior point methods maintain strict feasibility of iterates. They add a barrier function to the objective and slowly decrease its weight to zero. For positive (semidefinite) programming, $-\log(\det)$ is a popular choice [53, 54]. This work develops interior point methods for Euler equations that maintain feasibility (regularity) while preserving the long-time behavior of the solution.

Information geometric regularization. The negative log-barrier function of positive programming is also the negative entropy of the family of centered independent Gaussians, interpreting the optimization variable as a covariance matrix. As such, it defines a *dually flat information geometry* on the cone of positive-definite diagonal matrices [6, 1, 8]. The Hessian of the barrier function is the Riemannian metric while its gradient defines a notion of straight line [55, 1]. These so-called *dual geodesics* neither correspond to straight lines in the ordinary sense nor minimize the length defined by the Riemannian metric. But they *bend away* from the boundary of the positive-definite cone, thus preserving feasibility. By the same construction, any strictly convex barrier function ψ induces a dually flat geometry. For a linear objective function $\mathbf{x} \mapsto \mathbf{v}^T \mathbf{x}$, the iterates of interior point methods with barrier function ψ move along such a dual geodesic [1, Chapter 13.5] in direction \mathbf{v} . Using the barrier function ψ thus amounts to replacing ordinary straight lines with dual geodesics generated by ψ . This perspective extends beyond optimization problems and applies to characteristics of the Burgers equation, which are Euclidean straight lines in $(\bar{\Phi}, \Phi')$ -space.

Euclidean straight lines are dual geodesics defined by the barrier function

$$\psi_E(\Phi) := \psi_E(\bar{\Phi}, \Phi') := \frac{\bar{\Phi}^2 + \Phi'^2}{2} = \frac{\Phi(x_1)^2 + \Phi(x_2)^2}{2}.$$

Information geometric regularization modifies the Burgers and Euler equations by changing ψ to account for the positivity constraint on Φ' . For instance, we can choose

$$\psi(\Phi) := \psi(\bar{\Phi}, \Phi') := \psi_E + \alpha(-\log(\Phi')),$$

where $\alpha \geq 0$ modulates the regularization. **Figure 4** shows how the resulting characteristics approach the boundary of the feasible set, without leaving it.

2.3. Information Geometry in the infinite-dimensional setting.

From characteristics to diffeomorphisms. To obtain a Eulerian description of the modified equation, we have to extend the construction in **Figure 4** from two characteristics to an infinity of characteristics. Instead of keeping track of individual characteristics of the form $t \mapsto \bar{\Phi}_t(x)$, we keep track of the path $t \mapsto \bar{\Phi}_t$ in function space. Beginning with the seminal work of Arnold, the field of geometric hydrodynamics has studied fluid dynamics as geodesic curves on diffeomorphism manifolds [7]. Arnold, Ebin, and Marsden focused on inviscid and incompressible fluids that are described by geodesics on the manifold of volume-preserving diffeomorphisms [7, 30]. Similarly, the inviscid Burgers' and compressible Euler equations are solutions of the geodesic or Newton equations with respect to the L^2 metric on the manifold of general (not necessarily volume preserving) diffeomorphisms [45, 46]. This manifold is not geodesically complete under the L^2 metric, meaning some L^2 geodesics cannot continue indefinitely before leaving the manifold of diffeomorphisms. As $t \mapsto \bar{\Phi}_t$ reaches the boundary of the manifold, its spatial derivative $D\bar{\Phi}_t$ becomes singular and $\bar{\Phi}_t$ ceases to be differentiably invertible. In physical terms, the flow develops a shock.

Regularization on the diffeomorphism manifold. The regularization of geodesic curves of diffeomorphisms is analogous to that of characteristic curves as shown in **Figure 4**. For characteristic curves, new coordinates $(\bar{\Phi}, \Phi')$ are obtained by $\bar{\Phi} = (\Phi(x_1) + \Phi(x_2))/2$ and $\Phi' = (\Phi(x_1) - \Phi(x_2))/2$. For diffeomorphisms, we define $\bar{\Phi} := \int_{\mathbb{R}} (\Phi(x) - x) dx$ and $\Phi' := \partial_x \Phi$, with the latter being function-valued. The Euclidean barrier is $\psi_E := \frac{1}{2} \|\Phi(\cdot) - (\cdot)\|_{L^2}^2$, yielding the modified barrier

$$\psi(\Phi) = \psi_E(\Phi) + \alpha \int_{\mathbb{R}} (-\log(\partial_x \Phi)) dx.$$

Integration amounts to summing infinitely many barrier functions, each preventing a pair of characteristics from crossing, akin to barrier functions for polytopes [53].

2.4. From Burgers to Euler: The final equations.

A non-convex extension. Positivity of $\partial_x \Phi$ for equations on \mathbb{R} extends to positivity of the Jacobian determinant $\det(D\Phi)$ for equations on \mathbb{R}^d . This motivates using the log determinant barrier function of positive-definite programming,

$$\hat{\psi}(\Phi) := \psi(\Phi, \det D\Phi) := \psi_E(\Phi) + \alpha \int_{\mathbb{R}^d} (-\log \det(D\Phi)) dx.$$

Since $-\log \det$ is convex only on symmetric-positive matrices, $\hat{\psi}$ does not generate a dually flat geometry in the sense of [2]. Instead, we view the multivariate diffeomorphism manifold as a submanifold of the space of pairs (Φ, Φ') through the embedding $\Phi \mapsto (\Phi, \det(D\Phi))$. The ψ -geometry on the ambient space induces a geometry on the diffeomorphism manifold embedded into it that prevents the collapse of geodesics.

Pressure and external forces. Whereas Burgers' equation and its multidimensional analogs are geodesic equations on the diffeomorphism manifold, the compressible Euler and Navier-Stokes equations arise by adding forces to the geodesic equations [46], due to pressure, viscosity, and external forces acting on the gas. Adding these forces to dual geodesic equations yields regularizations of the Euler and Navier Stokes equations and numerous other systems including those listed in [46, Table 1]. For the sake of concreteness, this work focuses on the case of the barotropic Euler equation. For nonzero pressure, shock waves of entropy solutions have finite density and are thus not on the boundary of the diffeomorphism manifold. But jump discontinuities in the velocity cause the flow to leave the manifold instantaneously. Thus, the geodesically complete geometry defined by ψ also prevents the formation of jump discontinuities.

Euclidean description. We obtain the final regularized equation by converting the Lagrangian representation in terms of the deformation map Φ to a Eulerian description in terms of ρ and $\rho \mathbf{u}$ using $\mathbf{u}(\Phi(x)) := \dot{\Phi}(x)$ and $\rho(\Phi(x)) := (\det(D\Phi))^{-1}$. Using these definitions, we also note that $\int_{\mathbb{R}^d} -\log \det(D\Phi) dx = \int_{\mathbb{R}^d} \log(\rho) \rho dx$. The regularization term is the negative Shannon entropy of the mass distribution.

3. Derivation in the unidimensional case, using flat geometry.

Notation and Setting. We begin by deriving unidimensional information geometric regularization for general barrier functions ψ . A formal derivation is sufficient to obtain the regularized PDE. Thus, we will not discuss the technical complications that arise in the treatment of infinite-dimensional manifolds [62]. We consider problems on \mathbb{R}^d decaying at infinity and postpone the treatment of bounded domains and boundary values to future work. Using the ambient space $\mathcal{A} := \mathbf{I} + H^1(\mathbb{R}^d; \mathbb{R}^d)$ with \mathbf{I} the identity function on \mathbb{R}^d , $\mathcal{M} \subset \mathcal{A}$ denotes the diffeomorphism manifold. Capital Greek letters denote points on \mathcal{M} and capital Roman letters denote tangent vectors.

3.1. Derivation for abstract barrier ψ .

3.1.1. Exponential maps. Differential geometry distinguishes *points* $\Phi \in \mathcal{M}$ on a manifold from *directions* $U \in T_{\Phi}\mathcal{M}$ in the tangent space of \mathcal{M} at Φ . These two notions are connected by the *exponential map* $\text{Exp}_{(\Phi)}(U) \in \mathcal{M}$ that returns a new point in \mathcal{M} obtained by traveling, for a unit time interval, with initial velocity U , starting in Φ . For instance, we can use the Euclidean structure of \mathcal{A} to define the Exponential map $\text{Exp}_{(\Phi)}(U) = \Phi + U$. But any given manifold admits a multitude of exponential maps corresponding to different ways of continuing an initial velocity U to a path $t \mapsto \text{Exp}_{(p)}(tU)$. Paths of this form are called geodesics. Riemannian manifolds possess a so-called Levi-Civita exponential map generating locally length-minimizing geodesics. But geodesics of general exponential maps need not be length-minimizing.

3.1.2. The dual exponential map defined by the convex barrier ψ on \mathcal{M} is

$$\text{Exp}_{(\Phi)}^{\psi}(U) := \nabla \psi^{-1}(\nabla \psi(\Phi) + [D^2 \psi(\Phi)]U).$$

As shown in [Figure 5](#), $\text{Exp}_{(\Phi)}^{\psi}(U)$ is obtained from the Euclidean exponential map in the coordinate system given by $\nabla \psi$. It plays an important role in mirror descent

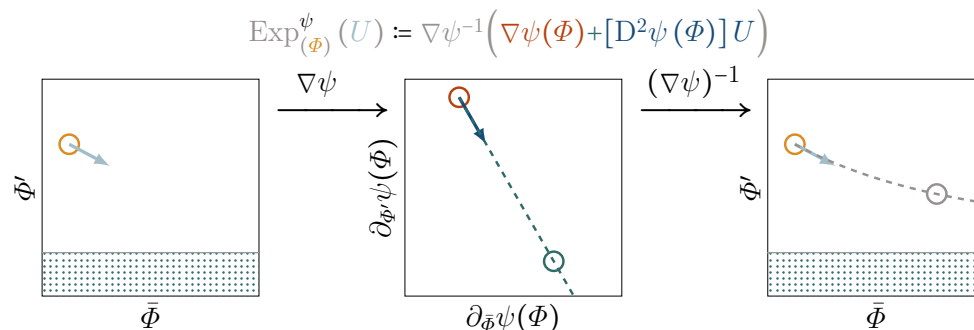


FIG. 5. The barrier function ψ defines a dual exponential map on \mathcal{M} through the Euclidean exponential map in the coordinate system given by $\nabla\psi$.

[54, 58, 61] and information geometry [6]. The dual exponential map on the probability simplex induced by the negative Shannon entropy $\psi(p) = \sum_{i=1}^n \log(p_i)p_i$ arises as the unique exponential map that is invariant under sufficient statistics, geodesically complete, and flat [20]. Many other barriers and their geometries arise from parametric families of probability distributions that are (at least formally) submanifolds of infinite-dimensional probability simplices [6, 33]. For instance, $\psi(\Theta) := \log \det \Theta$ is the entropy of the family $\{\mathcal{N}(0, \Theta) : \Theta \text{ is s.p.d.}\}$ of centered Gaussian distributions.

3.1.3. The dual equations of motion. The solution paths of an interior point method with barrier ψ are geodesics of Exp^ψ . We use this property to extend interior point methods to dynamical systems by replacing Euclidean geodesics

$$\bar{\Phi}_t := \text{Exp}_{(\bar{\Phi}_0)}^\psi(t\dot{\bar{\Phi}}_0) \quad \text{with dual geodesics} \quad \Phi_t := \text{Exp}_{(\Phi_0)}^\psi(t\dot{\Phi}_0).$$

We still need to account for forces due to, for instance, pressure or gravity. To this end, we take the second time derivative to deduce the equations of dual inertial motion

$$(3.1) \quad \ddot{\bar{\Phi}}_t + [D^2\psi(\bar{\Phi}_t)]^{-1} [D^3\psi(\bar{\Phi}_t)] (\dot{\bar{\Phi}}_t, \dot{\bar{\Phi}}_t) = 0.$$

In the Euclidean case, ψ is quadratic and the curvature term $D^3\psi$ vanishes, yielding Newton's first law. For forces $K(t, \bar{\Phi}_t, \dot{\bar{\Phi}}_t)$ the dual version of Newton's second law is

$$(3.2) \quad \ddot{\bar{\Phi}}_t + [D^2\psi(\bar{\Phi}_t)]^{-1} [D^3\psi(\bar{\Phi}_t)] (\dot{\bar{\Phi}}_t, \dot{\bar{\Phi}}_t) = K(t, \bar{\Phi}_t, \dot{\bar{\Phi}}_t).$$

3.2. Deriving the regularized PDE in the unidimensional case.

3.2.1. The logarithmic barrier function. We regularize the squared Euclidean norm with the negative logarithm, yielding

$$(3.3) \quad \psi(\Phi) = \frac{1}{2} \int_{\mathbb{R}} |\Phi(x) - x|^2 dx + \alpha \int_{\mathbb{R}} -\log \partial_x \Phi(x) dx.$$

The parameter α determines the strength of the regularization. The negative logarithm is a popular barrier function for optimization on the positive cone. It enforces positivity of the iterates and its *self-concordance* ensures rapid convergence of damped Newton minimization algorithms [53]. It is also the negative Shannon entropy of the Eulerian mass density $\rho(\Phi(x)) := (\det(D\Phi(x)))^{-1}$. Thus, it induces the unique Markov-invariant geometry on the manifold of mass distributions [20, 33]. We believe that these connections of ψ to mathematical programming and information geometry will aid the analysis of information geometric regularization in future work.

3.2.2. The modified equations in Lagrangian coordinates. To derive the modified equation, we want to specialize (3.2) to the barrier function ψ of (3.3). Computationally, this amounts to a function-valued version of

$$\left(\frac{(x-1)^2}{2} - \alpha \log(x)\right)''' = \left((x-1) - \alpha \frac{1}{x}\right)'' = \left(1 + \alpha \frac{1}{x^2}\right)' = \left(-\alpha \frac{2}{x^3}\right).$$

Taking the variation in direction U at Φ yields

$$[D\psi(\Phi)](U) = \int_{\mathbb{R}} (\Phi(x) - x)U(x) \, dx + \alpha \int_{\mathbb{R}} -\frac{\partial_x U(x)}{\partial_x \Phi(x)} \, dx$$

Computing the gradient with respect to the L^2 inner product yields

$$\nabla \psi(\Phi) = \Phi - x + \alpha \partial_x \left(\frac{1}{\partial_x \Phi}\right).$$

Likewise, the second variation is given by

$$[D^2\psi(\Phi)](U, V) = \int_{\mathbb{R}} U(x) \cdot V(x) \, dx + \alpha \int_{\mathbb{R}} \frac{\partial_x U(x) \cdot \partial_x V(x)}{(\partial_x \Phi(x))^2} \, dx,$$

and by using the L^2 inner product we obtain the linear map

$$[D^2\psi(\Phi)]: U \mapsto U - \alpha \cdot \partial_x \left(\frac{\partial_x U}{(\partial_x \Phi)^2}\right).$$

Finally, we compute the third variation as

$$[D^3\psi(\Phi)](U, V, W) = -2\alpha \int_{\mathbb{R}} \frac{\partial_x U(x) \cdot \partial_x V(x) \cdot \partial_x W(x)}{(\partial_x \Phi(x))^3} \, dx.$$

Again using the L^2 inner product, we obtain the quadratic map

$$[D^3\psi(\Phi, \Phi')]: (U, V) \mapsto 2\alpha \partial_x \left(\frac{\partial_x U \cdot \partial_x V}{(\partial_x \Phi)^3}\right)$$

Plugging the above into (3.2) results in the modified equation

$$\ddot{\Phi}_t + \left((\cdot) - \alpha \partial_x \left([\partial_x \Phi_t]^{-2} [\partial_x (\cdot)]\right)\right)^{-1} 2\alpha \partial_x \left([\partial_x \Phi_t]^{-3} [\partial_x \dot{\Phi}_t]^2\right) = K(t, \Phi_t, \dot{\Phi}_t).$$

Equivalently we can write

$$(3.4) \quad \left((\cdot) - \alpha \partial_x \left([\partial_x \Phi_t]^{-2} [\partial_x (\cdot)]\right)\right) (\ddot{\Phi}_t - K(t, \Phi_t, \dot{\Phi}_t)) = -2\alpha \partial_x \left([\partial_x \Phi_t]^{-3} [\partial_x \dot{\Phi}_t]^2\right).$$

3.2.3. The modified equations in Eulerian coordinates. We now write the Eulerian velocity field u as

$$\dot{\Phi}_t(x) =: u(\Phi_t(x)) \quad \Rightarrow \quad \ddot{\Phi}_t(x) = [\partial_x u(\Phi_t(x))] u(\Phi_t(x)) + \partial_t u(\Phi_t(x))$$

and the Eulerian density ρ as $\rho(\Phi_t(x)) = (\partial_x \Phi_t(x))^{-1}$. For $V := \ddot{\Phi}_t - K(t, \Phi_t, \dot{\Phi}_t)$ we integrate both sides of (3.4) against a vector field U , obtaining

$$\int_{\mathbb{R}} U \cdot \left(V - \alpha \partial_x \left([\partial_x \Phi_t]^{-2} [\partial_x V]\right)\right) \, dx = - \int_{\mathbb{R}} 2\alpha U \cdot \partial_x \left([\partial_x \Phi_t]^{-3} [\partial_x \dot{\Phi}_t]^2\right) \, dx.$$

Integrating by parts, we obtain

$$\int_{\mathbb{R}} U \cdot V + \alpha [\partial_x U] [\partial_x \Phi_t]^{-3} [\partial_x V] \, dx = \int_{\mathbb{R}} 2\alpha [\partial_x U] [\partial_x \Phi_t]^{-3} [\partial_x \dot{\Phi}_t]^2 \, dx.$$

We now perform a change of variables

$$\begin{aligned} & \int_{\mathbb{R}} \left(U \cdot V + \alpha [\partial_x U] [\partial_x \Phi_t]^{-2} [\partial_x V] \right) \circ \Phi_t^{-1} \cdot (\partial_x \Phi_t^{-1}) \, dx \\ &= \int_{\mathbb{R}} 2\alpha \left([\partial_x U] [\partial_x \Phi_t]^{-3} [\partial_x \dot{\Phi}_t]^2 \right) \circ \Phi_t^{-1} \cdot (\partial_x \Phi_t^{-1}) \, dx. \end{aligned}$$

Noting that $[\partial_x \dot{\Phi}_t] = [\partial_x u] \circ \Phi_t [\partial_x \Phi_t]$ and writing $U = \tilde{U} \circ \Phi$ and $V = \tilde{V} \circ \Phi$ yields

$$\int_{\mathbb{R}} (\tilde{U} \cdot \tilde{V} + \alpha [\partial_x \tilde{U}] [\partial_x \tilde{V}]) \rho \, dx = \int_{\mathbb{R}} 2\alpha [\partial_x \tilde{U}] [\partial_x u]^2 \rho \, dx.$$

Integrating by part once more, we obtain as before

$$\int_{\mathbb{R}} \tilde{U} \cdot \tilde{V} \rho - \tilde{U} \cdot \alpha \partial_x ([\partial_x \tilde{V}] \rho) \, dx = - \int_{\mathbb{R}} 2\alpha \tilde{U} \cdot \partial_x ([\partial_x u]^2 \rho) \, dx.$$

Using the fact that U and thus \tilde{U} was chosen fully general, we obtain

$$\partial_t u + [\partial_x u] u + ((\cdot) \rho - \alpha \partial_x (\rho [\partial_x (\cdot)]))^{-1} 2\alpha \partial_x ([\partial_x u]^2) = K(t, \Phi_t, \dot{\Phi}_t) \circ \Phi_t^{-1}.$$

which we combine with the transport equation $\partial_t \rho + \partial_x (u \rho) = 0$.

3.2.4. A regularized conservation law. To express the regularized equation in conservation form, we multiply with ρ and use the equation for mass conservation,

$$\partial_t (\rho u) + [\partial_x \rho] u^2 + u \rho (\partial_x u) + \rho [\partial_x u] u + 2\alpha \rho (\rho - \alpha \partial_x \rho \partial_x)^{-1} \partial_x (\rho [\partial_x u]^2) = K \circ \Phi_t^{-1}.$$

We now use the identity $\partial_x (\rho u \cdot u) \partial_x (\rho u) u + \rho u \partial_x (u)$ to conclude

$$\partial_t (\rho u) + \partial_x (\rho u^2) + 2\alpha \rho (\rho - \alpha \partial_x \rho \partial_x)^{-1} \partial_x (\rho [\partial_x u]^2) = K(t, \Phi_t, \dot{\Phi}_t) \circ \Phi_t^{-1}.$$

We now use the identity $(\mathcal{A}\mathcal{B})^{-1} = \mathcal{B}^{-1}\mathcal{A}^{-1}$ for linear operators \mathcal{A} and \mathcal{B} to obtain

$$\begin{aligned} & 2\alpha \rho (\rho - \alpha \partial_x \rho \partial_x)^{-1} \partial_x (\rho [\partial_x u]^2) = 2\alpha (\text{Id} - \alpha \partial_x \rho \partial_x \rho^{-1})^{-1} \partial_x (\rho [\partial_x u]^2) \\ &= 2\alpha (\partial_x^{-1} - \alpha \rho \partial_x \rho^{-1})^{-1} (\rho [\partial_x u]^2) = 2\alpha \partial_x \left((\text{Id} - \alpha \rho \partial_x \rho^{-1} \partial_x)^{-1} (\rho [\partial_x u]^2) \right) \\ &= 2\alpha \partial_x \left((\rho^{-1} - \alpha \partial_x \rho^{-1} \partial_x)^{-1} [\partial_x u]^2 \right). \end{aligned}$$

Setting $K(t, \Phi_t, \dot{\Phi}_t) \circ \Phi_t^{-1} = \partial_x P(\rho) - f$, the regularized Euler equation becomes

$$(3.5) \quad \begin{cases} \partial_t (\rho u) + \partial_x (\rho u^2 + P(\rho) + \Sigma) & = f \\ \partial_t \rho + \partial_x (\rho u) & = 0 \\ \Sigma \rho^{-1} - \alpha \partial_x (\rho^{-1} \partial_x \Sigma) & = 2\alpha [\partial_x u]^2. \end{cases}$$

4. Derivation in the multivariate case, using a nonlinear embedding.

4.1. The need for non-convex information geometry.

4.1.1. Shock formation in multidimensional problems. In the univariate setting, the only scenario for shock formation is the vanishing of the derivative $\partial_x \Phi_t$ of the deformation map. In $d > 1$ dimensions, any loss of invertibility of $D\Phi_t$ results in shock formation. The dimension of the null space of $D\Phi_t$ determines the dimension of the resulting shock singularity. The most common situation, a $(d - 1)$ -dimensional shock front, arises from $D\Phi_t$ having a one-dimensional null space normal to the shock front. Thus, our barrier function ψ needs to prevent any loss of invertibility of $D\Phi_t$.

4.1.2. The log determinantal barrier function. In mathematical programming, the natural generalization of the logarithmic barrier function to semidefinite programming is the log determinant barrier function [40]. Just like the logarithmic barrier function on the positive cone, it is convex and self-concordant on the cone of symmetric and positive-definite matrices, enabling the efficient implementation of homotopy methods. This suggests generalizing [section 3](#) by using the barrier

$$\hat{\psi}(\Phi) := \frac{1}{2} \int_{\mathbb{R}^d} \|\Phi - \text{Id}\|^2 dx + \alpha \int_{\mathbb{R}^d} (-\log \det(D\Phi)) dx.$$

4.1.3. Nonconvexity of $\hat{\psi}$. The problem with this approach is that the Jacobians of diffeomorphisms are generally not symmetric and thus $\hat{\psi}$ is not convex on \mathcal{M} and does not define a dually flat information geometry in the sense of [6]. Likewise, in mathematical elasticity, no convex energy functional can simultaneously be rotationally invariant and prevent the collapse of deformation maps [26]. The seminal work [9] overcomes this problem by introducing polyconvex energy functionals that are convex functions of Jacobian determinants. The weak continuity of the determinant allows applying the direct method of the calculus of variations to polyconvex problems [28].

4.1.4. Regularization by embedding. Inspired by the idea of polyconvexity, we introduce the map $\xi: \Phi \mapsto (\Phi, \det(D\Phi))$ that embeds the diffeomorphism manifold \mathcal{M} into the extended ambient space \mathcal{E} consisting of pairs (Φ, Φ') of deformation and Jacobian-determinant degrees of freedom. We define the barrier function ψ on \mathcal{E} as

$$\psi(\Phi, \Phi') := \frac{1}{2} \int_{\mathbb{R}^d} \|\Phi - \text{Id}\|^2 dx + \alpha \int_{\mathbb{R}^d} (-\log(\Phi')) dx.$$

This barrier function is convex and thus defines a dually flat information geometry on \mathcal{E} . The Riemannian metric defined by the Hessian of ψ and the embedding ξ induce an exponential map on \mathcal{M} that avoids the formation of shock singularities. We think that the weak continuity of ξ will aid the rigorous analysis of the resulting PDE.

4.2. Derivation for general embedding and potential.

Notation and Setting. We now derive information geometric regularization in the multidimensional setting. To this end, we consider the extended ambient space $\mathcal{E} := (\mathbf{I} + L^2(\mathbb{R}^d; \mathbb{R}^d)) \times L^{\log}(\mathbb{R}^d)$, where $L^{\log}(\mathbb{R}^d)$ denotes the space of positive and log-integrable functions on \mathbb{R}^d . We consider the diffeomorphism manifold $\mathcal{M} \hookrightarrow \mathcal{E}$ as a submanifold of \mathcal{E} , through the embedding $\xi: \Phi \mapsto (\Phi, \det(D\Phi))$. Our potential ψ will be defined on the extended ambient space \mathcal{E} . We denote by capital Greek letters points on the manifolds \mathcal{M} and \mathcal{E} and by capital Roman letters the elements of their

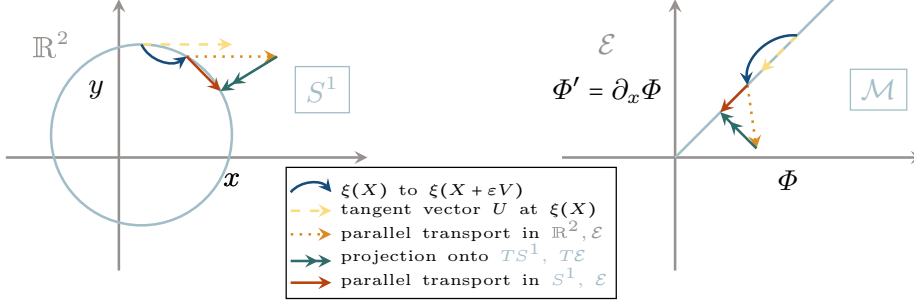


FIG. 6. **Parallel transport on submanifolds.** Parallel transport on a submanifold is parallel transport in the ambient manifold, followed by projection onto the tangent space of the submanifold. For $S^1 \hookrightarrow \mathbb{R}^2$, the difference between parallel transport on ambient and submanifold arises from the nonlinearity of the embedding ξ . In unidimensional IGR, ξ is affine but the parallel transport on the ambient space does not respect its linear structure, resulting in a difference between parallel transport on \mathcal{M} and \mathcal{E} . In multidimensional IGR, ξ is nonlinear and both of the above effects contribute.

tangent spaces. We denote elements of \mathcal{E} or its tangent spaces as (Φ, Φ') or (U, U') to distinguish the two degrees of freedom.

4.2.1. Exponential maps, geodesics, and parallel transport. In section 3, we derived dual equations of inertial motion (3.1) by taking derivatives of the dual exponential map. Equivalently, they can be defined via the dual *affine connection*

$$\Gamma_{\Phi}^{\psi}(U, V) := [\mathbb{D}^2\psi(\Phi)]^{-1} [\mathbb{D}^3\psi(\Phi)](U, V).$$

The affine connection $\Gamma_{\Phi}^{\psi}(U, \cdot)$ defines a correspondence between the tangent spaces $T_{\Phi}\mathcal{M}$ and $T_{\Phi+\varepsilon U}\mathcal{M}$ in infinitesimally nearby base points Φ and $\Phi + \varepsilon U$. It identifies the vector $V + \varepsilon \Gamma_{\Phi}^{\psi}(U, V)$ as the tangent vector in $T_{\Phi}\mathcal{M}$ corresponding to the tangent vector V in $T_{\Phi+\varepsilon U}\mathcal{M}$. Equivalently, we can think of the map $V \mapsto V - \varepsilon \Gamma_{\Phi}^{\psi}(U, V)$ from $T_{\Phi}\mathcal{M}$ to $T_{\Phi+\varepsilon U}\mathcal{M}$ as transporting a tangent vector $V \in T_{\Phi}\mathcal{M}$ an infinitesimal small distance in the direction εU , resulting in an element of $T_{\Phi+\varepsilon U}\mathcal{M}$. This procedure is called *parallel transport*. Solutions of dual equations of motion or geodesic equations

$$\ddot{\Phi}_t + \Gamma_{\Phi}^{\psi}(\dot{\Phi}_t, \dot{\Phi}_t) = 0$$

are therefore curves with velocities that are parallel transported along themselves.

4.2.2. Parallel transport on submanifolds. We now want to use the parallel transport on \mathcal{E} by ψ to induce a parallel transport on the submanifold $\mathcal{M} \hookrightarrow \mathcal{E}$ with embedding ξ . As outlined in [1, Section 5.10], we proceed in three steps to transport a tangent vector V from $T_{\Phi}\mathcal{M}$ to $T_{\Phi+\varepsilon U}\mathcal{M}$. We use the embedding ξ to identify V with the element $[\mathbb{D}\xi(\Phi)]V$ of the tangent space $T_{\xi(\Phi)}\mathcal{E}$ of the ambient manifold \mathcal{E} . We then parallel transport $[\mathbb{D}\xi(\Phi)]V$ in the ambient manifold \mathcal{E} to the point $\xi(\Phi + \varepsilon U)$, obtaining $(W, W') \in T_{\xi(\Phi+\varepsilon U)}\mathcal{E}$. Finally, we project (W, W') on the tangent space $T_{\Phi+\varepsilon U}\mathcal{M}$ via the Riemannian metric on \mathcal{E} given by the Hessian of ψ ,

$$\langle\langle (U, U'), (V, V') \rangle\rangle_{(\Phi, \Phi')} := [\mathbb{D}^2\psi(\Phi, \Phi')](U, U')(V, V').$$

This is the Fisher-Rao metric of a family of probability distributions with entropy ψ , the unique Riemannian metric invariant under Markov isomorphisms [20, 33].

4.2.3. Computing the induced parallel transport. Transporting $[\mathbb{D}\xi(\Phi)]V$ to $\xi(\Phi + \varepsilon U)$ yields, to leading order in ε ,

$$(W, W') \approx [\mathbb{D}\xi(\Phi)]V - \varepsilon [\mathbb{D}^2\psi(\xi(\Phi))]^{-1} [\mathbb{D}^3\psi(\xi(\Phi))] ([\mathbb{D}\xi(\Phi)]U, [\mathbb{D}\xi(\Phi)]V).$$

The projection X of (W, W') onto $T_{\Phi + \varepsilon U}\mathcal{M}$ satisfies, for all $Y \in T_{\Phi + \varepsilon U}\mathcal{M}$,

$$\langle\langle [\mathbb{D}\xi(\Phi + \varepsilon U)]Y, [\mathbb{D}\xi(\Phi + \varepsilon U)]X \rangle\rangle_{\xi(\Phi + \varepsilon U)} = \langle\langle [\mathbb{D}\xi(\Phi + \varepsilon U)]Y, (W, W') \rangle\rangle_{\xi(\Phi + \varepsilon U)}.$$

Using the L^2 inner product, we can view $[\mathbb{D}^2\psi]$ as a linear map from \mathcal{E} to itself, with

$$\langle\langle (U, U'), (V, V') \rangle\rangle_{(\Phi, \Phi')} = \langle\langle (U, U'), [\mathbb{D}^2\psi(\Phi, \Phi')] (V, V') \rangle\rangle_{L^2}.$$

Denoting the L^2 -adjoint of $[\mathbb{D}\xi(\Phi + \varepsilon U)]$ as $[\mathbb{D}\xi(\Phi + \varepsilon U)]^*$, we obtain

$$\begin{aligned} X &\approx ([\mathbb{D}\xi(\Phi + \varepsilon U)]^* [\mathbb{D}^2\psi(\xi(\Phi + \varepsilon U))] [\mathbb{D}\xi(\Phi + \varepsilon U)])^{-1} \\ &\quad [\mathbb{D}\xi(\Phi + \varepsilon U)]^* [\mathbb{D}^2\psi(\Phi + \varepsilon U)] \\ &\quad \left([\mathbb{D}\xi(\Phi)]V - \varepsilon [\mathbb{D}^2\psi(\xi(\Phi))]^{-1} [\mathbb{D}^3\psi(\xi(\Phi))] ([\mathbb{D}\xi(\Phi)]U, [\mathbb{D}\xi(\Phi)]V) \right). \end{aligned}$$

To order ε^0 , we have $X = V$. In order to compute the first-order approximation of X in ε , we compute the derivative of the right-hand side. To simplify the notation, we define $\beta_\Phi := [\mathbb{D}\xi(\Phi)]$ and $\gamma_\Phi := [\mathbb{D}^2\psi(\xi(\Phi))]$. We compute

$$\begin{aligned} &\left. \frac{d}{d\varepsilon} \right|_{\varepsilon=0} (\beta_{\Phi + \varepsilon U}^* \gamma_{\Phi + \varepsilon U} \beta_{\Phi + \varepsilon U})^{-1} \beta_{\Phi + \varepsilon U}^* \gamma_{\Phi + \varepsilon U} (\beta_\Phi V - \varepsilon \gamma_\Phi^{-1} [\mathbb{D}^3\psi(\xi(\Phi))] (\beta_\Phi U, \beta_\Phi V)) \\ &= -(\beta_\Phi^* \gamma_\Phi \beta_\Phi)^{-1} \left[\left. \frac{d}{d\varepsilon} \right|_{\varepsilon=0} (\beta_{\Phi + \varepsilon U}^* \gamma_{\Phi + \varepsilon U} \beta_{\Phi + \varepsilon U}) \right] (\beta_\Phi^* \gamma_\Phi \beta_\Phi)^{-1} \beta_\Phi^* \gamma_\Phi \beta_\Phi V \\ &\quad + (\beta_\Phi^* \gamma_\Phi \beta_\Phi)^{-1} \left[\left. \frac{d}{d\varepsilon} \right|_{\varepsilon=0} \beta_{\Phi + \varepsilon U}^* \gamma_{\Phi + \varepsilon U} \right] \beta_\Phi V \\ &\quad - (\beta_\Phi^* \gamma_\Phi \beta_\Phi)^{-1} \beta_\Phi^* \gamma_\Phi \gamma_\Phi^{-1} [\mathbb{D}^3\psi(\xi(\Phi))] (\beta_\Phi U, \beta_\Phi V) \\ &= -(\beta_\Phi^* \gamma_\Phi \beta_\Phi)^{-1} (\beta_\Phi^* \gamma_\Phi [\mathbb{D}^2\xi(\Phi)] (U, V) + \beta_\Phi^* \gamma_\Phi \gamma_\Phi^{-1} [\mathbb{D}^3\psi(\xi(\Phi))] (\beta_\Phi U, \beta_\Phi V)) \end{aligned}$$

In summary, we obtain to first order in ε that

$$\begin{aligned} X &\approx V - \varepsilon ([\mathbb{D}\xi(\Phi)]^* [\mathbb{D}^2\psi(\xi(\Phi))] [\mathbb{D}\xi(\Phi)])^{-1} [\mathbb{D}\xi(\Phi)]^* [\mathbb{D}^2\psi(\xi(\Phi))] \\ &\quad \left([\mathbb{D}^2\xi(\Phi)] (U, V) + [\mathbb{D}^2\psi(\Phi)]^{-1} [\mathbb{D}^3\psi(\xi(\Phi))] ([\mathbb{D}\xi(\Phi)]U, [\mathbb{D}\xi(\Phi)]V) \right). \end{aligned}$$

Rewriting this result in terms of an affine connection, we obtain

$$\begin{aligned} \Gamma_\Phi^{\psi, \xi} (U, V) &= ([\mathbb{D}\xi(\Phi)]^* [\mathbb{D}^2\psi(\xi(\Phi))] [\mathbb{D}\xi(\Phi)])^{-1} [\mathbb{D}\xi(\Phi)]^* [\mathbb{D}^2\psi(\xi(\Phi))] \\ &\quad \left([\mathbb{D}^2\xi(\Phi)] (U, V) + [\mathbb{D}^2\psi(\Phi)]^{-1} [\mathbb{D}^3\psi(\xi(\Phi))] ([\mathbb{D}\xi(\Phi)]U, [\mathbb{D}\xi(\Phi)]V) \right). \end{aligned}$$

Note that the two summands in the above formula correspond to the two separate contributions to the affine connection, as illustrated in [Figure 6](#). The first summand arises from the nonlinearity (with respect to the vector space structure of \mathcal{E}) of the embedding ξ . This is akin to the curvature of a $(d-1)$ -sphere arising from the

nonlinearity of its embedding into \mathbb{R}^d . The second summand arises from the dual parallel transport on \mathcal{E} not respecting the vector space structure of \mathcal{E} . It induces a nontrivial parallel transport even for $d = 1$, where ξ is linear. In this case, it gives rise to the equations derived in [section 3](#).

4.3. The geodesic equation in Lagrangian form. We now plug in ξ and ψ and compute $\Gamma^{\psi, \xi}$, in order to derive the equation of inertial motion. The quadratic form associated with $(D^2\psi)$ is given by

$$[D^2\psi(\Phi, \Phi')]((U, U'), (V, V')) = \int_{\mathbb{R}^d} \langle U, V \rangle dx + \alpha \int_{\mathbb{R}^d} \frac{U'V'}{(\Phi')^2} dx$$

and using the L^2 inner product on \mathcal{E} , we obtain the linear map

$$[D^2\psi(\Phi, \Phi')] (U, U') = \left(U, \alpha \frac{U'}{(\Phi')^2} \right).$$

Similarly, we obtain the cubic form of the third derivative as

$$[D^3\psi(\Phi, \Phi')]((U, U'), (V, V'), (W, W')) = -2\alpha \int_{\mathbb{R}^d} \frac{U'V'W'}{(\Phi')^3} dx$$

and the resulting quadratic map

$$[D^3\psi(\Phi, \Phi')]((U, U'), (V, V')) = \left(0, -2\alpha \frac{U'V'}{(\Phi')^3} \right).$$

Similarly, using Jacobi's formula, we can compute the map

$$[D\xi(\Phi)]U = \left(U, \det(D\Phi) \operatorname{tr}([D\Phi]^{-1}[DU]) \right).$$

To compute its adjoint, we multiply with (W, W') and integrate

$$\langle (W, W'), [D\xi(\Phi)]U \rangle_{L^2} = \int_{\mathbb{R}^d} \langle U, W \rangle dx + \int_{\mathbb{R}^d} W' \det(D\Phi) \operatorname{tr}([D\Phi]^{-1}[DU]) dx.$$

Letting $\bar{V} := [D\xi(\Phi)]^*(W, W')$, we have, for $\downarrow \operatorname{div}$ the column-wise divergence,

$$\begin{aligned} \int_{\mathbb{R}^d} \langle \bar{V}, U \rangle dx &= \int_{\mathbb{R}^d} \langle U, W \rangle dx + \int_{\mathbb{R}^d} W' \det(D\Phi) \operatorname{tr}([D\Phi]^{-1}[DU]) dx \\ &= \int_{\mathbb{R}^d} \left\langle U, W - \downarrow \operatorname{div} \left(W' \det(D\Phi) [D\Phi]^{-1} \right) \right\rangle dx, \end{aligned}$$

resulting in

$$[D\xi(\Phi)]^*(W, W') = W - \downarrow \operatorname{div} \left(W' \det(D\Phi) [D\Phi]^{-1} \right).$$

This allows computing the second derivative $[\mathbf{D}\xi(\Phi)](U, V)$ of ξ as

$$\begin{aligned} [\mathbf{D}^2\xi(\Phi)](U, V) &= \frac{d}{d\varepsilon} \Big|_{\varepsilon=0} \left[\mathbf{D}\xi(\Phi + \varepsilon V) \right] U \\ &= (0, \det(\mathbf{D}\Phi) \operatorname{tr}([\mathbf{D}\Phi]^{-1}[\mathbf{D}U]) \operatorname{tr}([\mathbf{D}\Phi]^{-1}[\mathbf{D}V])) \\ &\quad - (0, \det(\mathbf{D}\Phi) \operatorname{tr}([\mathbf{D}\Phi]^{-1}[\mathbf{D}U][\mathbf{D}\Phi]^{-1}[\mathbf{D}V])). \end{aligned}$$

We now derive the dual equations of inertial motion $\ddot{\Phi}_t + \Gamma_{\dot{\Phi}_t}^{\psi, \xi}(\dot{\Phi}_t, \dot{\Phi}_t) = 0$ in the form

$$\begin{aligned} [\mathbf{D}\xi(\Phi)]^* [\mathbf{D}^2\psi(\xi(\Phi))] [\mathbf{D}\xi(\Phi)] \ddot{\Phi} &= [\mathbf{D}\xi(\Phi)]^* [\mathbf{D}^2\psi(\xi(\Phi))] \\ &\quad \left([\mathbf{D}^2\xi(\Phi)](\dot{\Phi}, \dot{\Phi}) + [\mathbf{D}^2\psi(\Phi)]^{-1} [\mathbf{D}^3\psi(\xi(\Phi))]([\mathbf{D}\xi(\Phi)]\dot{\Phi}, [\mathbf{D}\xi(\Phi)]\dot{\Phi}) \right). \end{aligned}$$

We stop tracking the t dependence explicitly to simplify notation. We first compute

$$\begin{aligned} &[\mathbf{D}\xi(\Phi)]^* [\mathbf{D}^2\psi(\xi(\Phi))] [\mathbf{D}\xi(\Phi)] \ddot{\Phi} \\ &= [\mathbf{D}\xi(\Phi)]^* [\mathbf{D}^2\psi(\xi(\Phi))] (\ddot{\Phi}, \det(\mathbf{D}\Phi) \operatorname{tr}([\mathbf{D}\Phi]^{-1}[\mathbf{D}\ddot{\Phi}])) \\ &= [\mathbf{D}\xi(\Phi)]^* \left(\ddot{\Phi}, -\alpha \operatorname{tr}([\mathbf{D}\Phi]^{-1}[\mathbf{D}\ddot{\Phi}]) / \det(\mathbf{D}\Phi) \right) \\ &= \ddot{\Phi} - \alpha \operatorname{div}^\downarrow \left(\operatorname{tr}([\mathbf{D}\Phi]^{-1}[\mathbf{D}\ddot{\Phi}]) [\mathbf{D}\Phi]^{-1} \right). \end{aligned}$$

We next compute

$$\begin{aligned} &\left([\mathbf{D}^2\xi(\Phi)](\dot{\Phi}, \dot{\Phi}) + [\mathbf{D}^2\psi(\Phi)]^{-1} [\mathbf{D}^3\psi(\xi(\Phi))]([\mathbf{D}\xi(\Phi)]\dot{\Phi}, [\mathbf{D}\xi(\Phi)]\dot{\Phi}) \right) \\ &= (0, \det(\mathbf{D}\Phi) \operatorname{tr}([\mathbf{D}\Phi]^{-1}[\mathbf{D}\dot{\Phi}]) \operatorname{tr}([\mathbf{D}\Phi]^{-1}[\mathbf{D}\dot{\Phi}])) \\ &\quad - (0, \det(\mathbf{D}\Phi) \operatorname{tr}([\mathbf{D}\Phi]^{-1}[\mathbf{D}\dot{\Phi}][\mathbf{D}\Phi]^{-1}[\mathbf{D}\dot{\Phi}])) \\ &\quad - (0, 2 \det(\mathbf{D}\Phi) \operatorname{tr}([\mathbf{D}\Phi]^{-1}[\mathbf{D}\dot{\Phi}]) \operatorname{tr}([\mathbf{D}\Phi]^{-1}[\mathbf{D}\dot{\Phi}])) \\ &= - (0, \det(\mathbf{D}\Phi) \operatorname{tr}([\mathbf{D}\Phi]^{-1}[\mathbf{D}\dot{\Phi}][\mathbf{D}\Phi]^{-1}[\mathbf{D}\dot{\Phi}])) \\ &\quad - (0, \det(\mathbf{D}\Phi) \operatorname{tr}([\mathbf{D}\Phi]^{-1}[\mathbf{D}\dot{\Phi}]) \operatorname{tr}([\mathbf{D}\Phi]^{-1}[\mathbf{D}\dot{\Phi}])). \end{aligned}$$

Plugging this into the dual equations of motion yields, for $\operatorname{tr}^2(\cdot)$ the squared trace,

$$\begin{aligned} \ddot{\Phi} - \alpha \operatorname{div}^\downarrow \left(\operatorname{tr}([\mathbf{D}\Phi]^{-1}[\mathbf{D}\ddot{\Phi}]) [\mathbf{D}\Phi]^{-1} \right) &= -\alpha \operatorname{div}^\downarrow \left(\operatorname{tr}([\mathbf{D}\Phi]^{-1}[\mathbf{D}\dot{\Phi}]^2) [\mathbf{D}\Phi]^{-1} \right) \\ &\quad - \alpha \operatorname{div}^\downarrow \left(\operatorname{tr}^2([\mathbf{D}\Phi]^{-1}[\mathbf{D}\dot{\Phi}]) [\mathbf{D}\Phi]^{-1} \right). \end{aligned}$$

4.4. In Eulerian coordinates. We now write the Eulerian velocity field \mathbf{u} as

$$\dot{\Phi}(x) =: \mathbf{u}(\Phi(x)) \quad \Rightarrow \quad \ddot{\Phi}(x) = [\mathbf{D}\mathbf{u}(\Phi(x))] \mathbf{u}(\Phi(x)) + \partial_t \mathbf{u}(\Phi(x))$$

and the Eulerian density ρ as $\rho(\Phi(x)) = (\det(\mathbf{D}\Phi(x)))^{-1}$. We integrate both sides of the dual equations of motion against a vector field V , obtaining

$$\begin{aligned} &\int_{\mathbb{R}^d} \left\langle V, \left(\ddot{\Phi} - \alpha \operatorname{div}^\downarrow \left(\operatorname{tr}([\mathbf{D}\Phi]^{-1}[\mathbf{D}\ddot{\Phi}]) [\mathbf{D}\Phi]^{-1} \right) \right) \right\rangle dx \\ &= -\alpha \int_{\mathbb{R}^d} \left\langle V, \operatorname{div}^\downarrow \left(\operatorname{tr}([\mathbf{D}\Phi]^{-1}[\mathbf{D}\dot{\Phi}]^2) [\mathbf{D}\Phi]^{-1} + \operatorname{tr}^2([\mathbf{D}\dot{\Phi}][\mathbf{D}\Phi]^{-1}) [\mathbf{D}\Phi]^{-1} \right) \right\rangle dx \end{aligned}$$

Integrating by parts, we obtain

$$\begin{aligned} & \int_{\mathbb{R}^d} \langle V, \ddot{\Phi} \rangle + \alpha \operatorname{tr} ([DV][D\Phi]^{-1}) \operatorname{tr} ([D\Phi]^{-1}[D\ddot{\Phi}]) \, dx \\ &= \alpha \int_{\mathbb{R}^d} \operatorname{tr} ([DV][D\Phi]^{-1}) \left(\operatorname{tr} ([D\Phi]^{-1}[D\dot{\Phi}]^2) + \operatorname{tr}^2 ([D\dot{\Phi}][D\Phi]^{-1}) \right) \, dx. \end{aligned}$$

We now plug in the definition of \mathbf{u} , replacing $\dot{\Phi}$ and $\ddot{\Phi}$ to obtain

$$\begin{aligned} & \int_{\mathbb{R}^d} \langle V, [[D\mathbf{u}]\mathbf{u} + \partial_t \mathbf{u}] \circ \Phi \rangle + \alpha \operatorname{tr} ([DV][D\Phi]^{-1}) \operatorname{tr} ([D([D\mathbf{u}]\mathbf{u} + \partial_t \mathbf{u})] \circ \Phi) \, dx \\ &= \alpha \int_{\mathbb{R}^d} \operatorname{tr} ([DV][D\Phi]^{-1}) \left(\operatorname{tr} ([D\mathbf{u}]^2 \circ \Phi) + \operatorname{tr}^2 ([D\mathbf{u}] \circ \Phi) \right) \, dx. \end{aligned}$$

We now write $V(x) = \tilde{V}(\Phi(x))$ to obtain

$$\begin{aligned} & \int_{\mathbb{R}^d} \langle \tilde{V} \circ \Phi, [[D\mathbf{u}]\mathbf{u} + \partial_t \mathbf{u}] \circ \Phi \rangle + \alpha \operatorname{tr} ([D\tilde{V}] \circ \Phi) \operatorname{tr} ([D([D\mathbf{u}]\mathbf{u} + \partial_t \mathbf{u})] \circ \Phi) \, dx \\ &= \alpha \int_{\mathbb{R}^d} \operatorname{tr} ([D\tilde{V}] \circ \Phi) \left(\operatorname{tr} ([D\mathbf{u}]^2 \circ \Phi) + \operatorname{tr}^2 ([D\mathbf{u}] \circ \Phi) \right) \, dx. \end{aligned}$$

We now perform a transformation of variables with Φ^{-1} , resulting in multiplication with $\det([D\Phi^{-1}]) = \det([D\Phi])^{-1} \circ \Phi^{-1}(x) = \rho(x)$,

$$\begin{aligned} & \int_{\mathbb{R}^d} \langle \tilde{V}, [[D\mathbf{u}]\mathbf{u} + \partial_t \mathbf{u}] \rho \rangle + \alpha \operatorname{tr} ([D\tilde{V}]) \operatorname{tr} ([D([D\mathbf{u}]\mathbf{u} + \partial_t \mathbf{u})]) \rho \, dx \\ &= \alpha \int_{\mathbb{R}^d} \operatorname{tr} ([D\tilde{V}]) \left(\operatorname{tr} ([D\mathbf{u}]^2) + \operatorname{tr}^2 ([D\mathbf{u}]) \right) \rho \, dx. \end{aligned}$$

We again integrate by parts, obtaining

$$\begin{aligned} & \int_{\mathbb{R}^d} \left\langle \tilde{V}, [[D\mathbf{u}]\mathbf{u} + \partial_t \mathbf{u}] \rho - \alpha \operatorname{div}^\downarrow (\operatorname{tr} (D([D\mathbf{u}]\mathbf{u} + \partial_t \mathbf{u})) \rho \mathbf{I}) \right\rangle \\ &= -\alpha \int_{\mathbb{R}^d} \left\langle \tilde{V}, \operatorname{div}^\downarrow (\operatorname{tr} ([D\mathbf{u}]^2) \rho \mathbf{I} + \operatorname{tr}^2 ([D\mathbf{u}]) \rho \mathbf{I}) \right\rangle \, dx. \end{aligned}$$

The general choice of \tilde{V} and the fundamental lemma of the calculus of variations yield

$$\left((\cdot) \rho - \alpha \operatorname{div}^\downarrow (\rho \operatorname{tr} (D(\cdot)) \mathbf{I}) \right) ([D\mathbf{u}]\mathbf{u} + \partial_t \mathbf{u}) = -\alpha \operatorname{div}^\downarrow (\operatorname{tr} ([D\mathbf{u}]^2) \rho \mathbf{I} + \operatorname{tr}^2 ([D\mathbf{u}]) \rho \mathbf{I}).$$

All matrix divergences above are taken over multiples of the identity matrix. Thus, we can safely replace them with row-wise divergences, obtaining

$$([D\mathbf{u}]\mathbf{u} + \partial_t \mathbf{u}) = -\alpha \left((\cdot) \rho - \alpha \operatorname{div}^\rightarrow (\rho \operatorname{tr} (D(\cdot)) \mathbf{I}) \right)^{-1} \operatorname{div}^\rightarrow (\operatorname{tr} ([D\mathbf{u}]^2) \rho \mathbf{I} + \operatorname{tr}^2 ([D\mathbf{u}]) \rho \mathbf{I}).$$

We multiply both sides with ρ and apply the conservation of mass to obtain

$$\begin{aligned} \partial_t (\rho \mathbf{u}) + \operatorname{div}^\rightarrow (\rho \mathbf{u} \otimes \mathbf{u}) &= -\alpha \rho \left((\cdot) \rho - \alpha \operatorname{div}^\rightarrow (\rho \operatorname{tr} (D(\cdot)) \mathbf{I}) \right)^{-1} \\ &\quad \operatorname{div}^\rightarrow (\operatorname{tr} ([D\mathbf{u}]^2) \rho \mathbf{I} + \operatorname{tr}^2 ([D\mathbf{u}]) \rho \mathbf{I}). \end{aligned}$$

4.4.1. In conservation form. We now want to bring the regularized equations in conservation form. As in [subsection 3.2.4](#), we pull divergences and multiplications with ρ through the inverse to obtain

$$\begin{aligned}
& -\alpha\rho\left((\cdot)\rho - \alpha\vec{\text{div}}(\rho\text{tr}(\text{D}(\cdot))\mathbf{I})\right)^{-1}\vec{\text{div}}(\text{tr}([\text{Du}]^2)\rho\mathbf{I} + \text{tr}^2([\text{Du}])\rho\mathbf{I}) \\
&= -\alpha\left((\cdot) - \alpha\vec{\text{div}}(\rho\text{tr}(\text{D}(\rho^{-1}(\cdot)))\mathbf{I})\right)^{-1}\vec{\text{div}}(\text{tr}([\text{Du}]^2)\rho\mathbf{I} + \text{tr}^2([\text{Du}])\rho\mathbf{I}) \\
&= -\alpha\left(\vec{\text{div}}^{-1}(\cdot) - \alpha\rho\text{tr}(\text{D}(\rho^{-1}(\cdot)))\mathbf{I}\right)^{-1}(\text{tr}([\text{Du}]^2)\rho\mathbf{I} + \text{tr}^2([\text{Du}])\rho\mathbf{I}) \\
&= -\alpha\vec{\text{div}}\left((\cdot) - \alpha\rho\text{tr}\left(\text{D}\left(\rho^{-1}\vec{\text{div}}(\cdot)\right)\right)\mathbf{I}\right)^{-1}(\text{tr}([\text{Du}]^2)\rho\mathbf{I} + \text{tr}^2([\text{Du}])\rho\mathbf{I}) \\
&= -\alpha\vec{\text{div}}\left(\rho^{-1}(\cdot) - \alpha\text{tr}\left(\text{D}\left(\rho^{-1}\vec{\text{div}}(\cdot)\right)\right)\mathbf{I}\right)^{-1}(\text{tr}([\text{Du}]^2)\mathbf{I} + \text{tr}^2([\text{Du}])\mathbf{I}).
\end{aligned}$$

In other words, the additional momentum flux satisfies

$$\rho^{-1}\mathbf{F} - \alpha\text{tr}\left(\text{D}\left(\rho^{-1}\vec{\text{div}}\mathbf{F}\right)\right)\mathbf{I} = -\alpha(\text{tr}([\text{Du}]^2)\mathbf{I} + \text{tr}^2([\text{Du}])\mathbf{I}).$$

It follows that \mathbf{F} is a multiple of the identity of the form $\mathbf{F} = \Sigma\mathbf{I}$, resulting in

$$\rho^{-1}\Sigma - \alpha\text{tr}(\text{D}(\rho^{-1}\nabla\Sigma)) = -\alpha(\text{tr}([\text{Du}]^2) + \text{tr}^2([\text{Du}])).$$

The trace of the Jacobian is just the (vector) divergence, resulting in

$$\rho^{-1}\Sigma - \alpha\text{div}(\rho^{-1}\nabla\Sigma) = -\alpha(\text{tr}([\text{Du}]^2) + \text{tr}^2([\text{Du}])).$$

After adding the pressure and external forces, this yields the information geometric regularization of the multidimensional barotropic Euler equation

$$(4.1) \quad \begin{cases} \partial_t \begin{pmatrix} \rho\mathbf{u} \\ \rho \end{pmatrix} + \vec{\text{div}} \begin{pmatrix} \rho\mathbf{u} \otimes \mathbf{u} + (P(\rho) + \Sigma)\mathbf{I} \\ \rho\mathbf{u} \end{pmatrix} = \begin{pmatrix} \mathbf{f} \\ 0 \end{pmatrix} \\ \rho^{-1}\Sigma - \alpha\text{div}(\rho^{-1}\nabla\Sigma) = \alpha(\text{tr}^2([\text{Du}]) + \text{tr}([\text{Du}]^2)). \end{cases}$$

5. Numerical experiments.

5.1. Overview. The numerical experiments in this section serve the dual purpose of illustrating the behavior of solutions to the modified equations and providing proof of the concept of using the latter for numerical purposes. We emphasize that the results in this section are not yet meant to be fair comparisons to the state-of-the-art in simulating compressible flows. Such a comparison requires comparison with stronger baselines (such as (W)ENO schemes) and the combined consideration of the different practical aspects such as computational cost, memory, and robustness. This is beyond the scope of this work and will be addressed in the future. We focus on Lax-Friedrichs and Lax-Wendroff methods as classical examples of the tradeoff between dissipation and Gibbs oscillations that is at the heart of all shock capturing.

5.2. The unidimensional case. We begin with an application to the unidimensional Euler equation. We use the pressure $P(\rho) = \rho^{1.4}$ and compare the solutions obtained by the Lax-Friedrichs (LF) scheme, the Richtmyer Lax-Wendroff (LW)

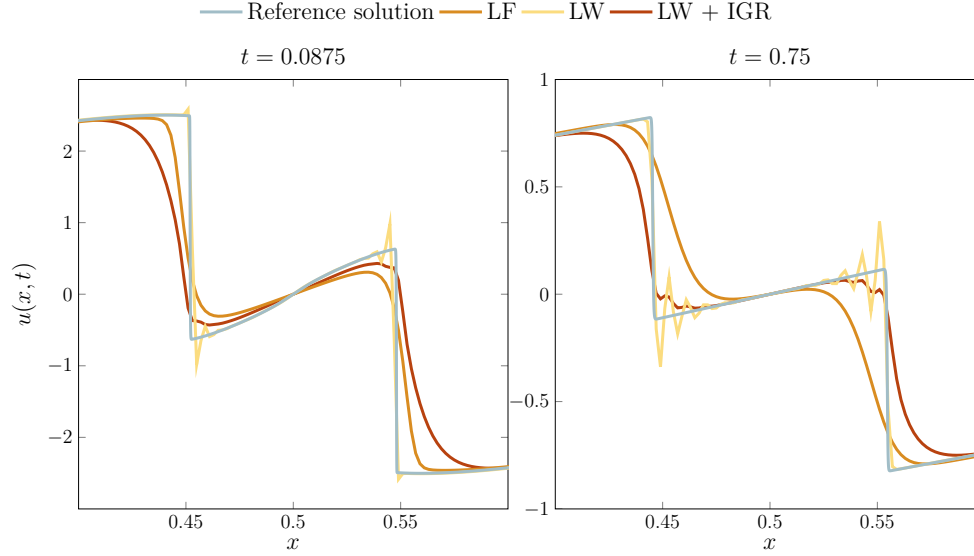


FIG. 7. **IGR on Euler:** Richtmyer Lax-Wendroff (LW) with information geometric regularization (IGR) avoids Gibbs oscillations in LW and the oversmoothing of Lax-Friedrichs (LF).

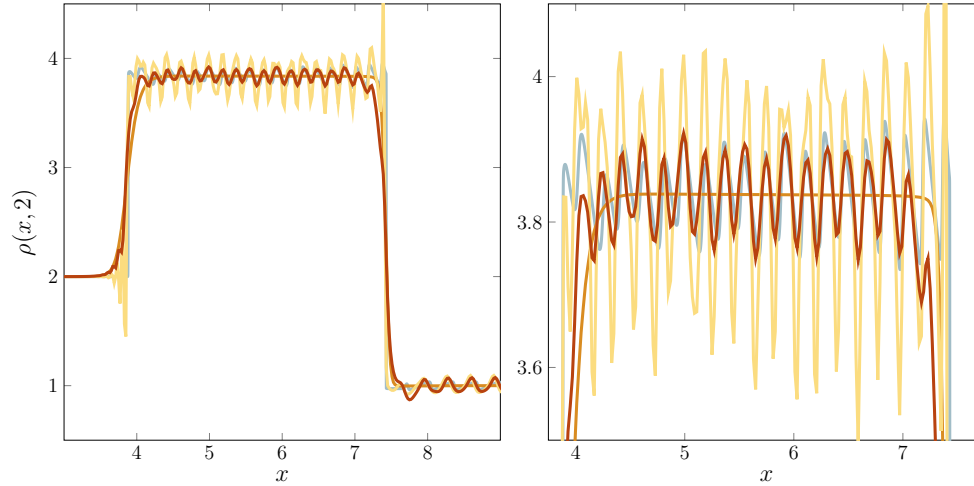


FIG. 8. **Interaction of shock and sound waves:** Information geometric regularization (IGR) with Lax-Wendroff (LW) correctly predicts the magnitude of the sound waves. Plain LW overestimates them while Lax-Friedrichs (LF) underestimates them.

scheme [48], and the LW scheme applied to (3.5) with $\alpha = 20(\Delta x)^2$ (LW + IGR). As is well known, the viscous regularization of LF causes excessive smoothness and the dispersive errors of LW cause spurious “Gibbs” oscillations near shocks. We are testing the hypothesis IGR can avoid these Gibbs oscillations by ensuring that the underlying continuous problem has a regular solution without adding excessive smoothing. We compute Σ by Gaussian elimination, at computational cost linear in the problem size.

5.2.1. Sine wave initial condition. For our first experiment, we choose initial conditions $u(x, 0) = 3 \sin(2\pi x)$, $\rho(x, 0) \equiv 1$, discretize the domain $[0, 1]$ with 500 grid points and use periodic boundary conditions. As shown in Figure 7, LW + IGR avoids

both the excessive dissipation of LF and the Gibbs oscillations of LW. We compare to a reference solution obtained by Lax-Friedrichs with 2×10^4 grid points.

5.2.2. Interaction of shock and sound waves. We next consider the problem

$$u(x, 0) \approx \begin{cases} 3, & \text{if } x < 2, \\ 0, & \text{else,} \end{cases} \quad \rho(x, 0) \approx \begin{cases} 2, & \text{if } x < 2 \\ 1 + 0.2 \sin(2\pi(25x)/8), & \text{if } 2 < x < 10, \\ 1, & \text{else,} \end{cases}$$

that features the interaction of a right-moving shock wave and a left-moving sound wave. We discretize the domain $[0, 10]$ using 500 points and add boundary padding equal to $(u(\cdot, 0), \rho(\cdot, 0))$. We use smooth cut-off functions for the transitions at $x = 2$ and at the wraparound of our periodic boundary conditions. We compare LF, LW, and LW + IGR to a reference solution computed with LF using 4×10^4 points on $[0, 10]$. As shown in [Figure 8](#), once the two waves interact, LF completely damps out the sound wave while LW greatly overestimates its magnitude. LW + IGR correctly estimates the sound wave's magnitude.

5.3. The multidimensional case. We now investigate the two-dimensional version of [\(4.1\)](#). We use the pressure $P(\rho) = \rho^{1.4}$ and multidimensional variants of the Lax-Friedrichs (LF) and Richtmyer Lax-Wendroff (LW) schemes. LW without IGR broke down with negative densities, which is why we only show LW + IGR. To improve the efficiency of LF and LW + IGR, we integrate the resulting fluxes into fourth and second-order Runge-Kutta (RK) methods, respectively. The elliptic problem defining Σ is solved using Jacobi iteration [\[60\]](#), with the previous solution as a warm start. Except for [Figure 14](#) that explores impractically large α , all results in this section are computed using a single Jacobi sweep per flux computation.

5.3.1. Blast wave interaction. We begin by simulating the interactions of three blast wave in $[0, 0.72] \times [0, 1.2]$, with periodic boundary conditions. The initial conditions are $u(x, y, 0) \equiv 0$ and $\rho(x, y, 0) = 1 + 0.6\eta_1(x, y) + 1.2\eta_2(x, y) + 0.5\eta_3(x, y)$, where the η_i are Gaussian densities with means $((0.2, 0.2), (0.4, 0.7), (0.3, 1.05))$ and standard deviations $(0.05, 0.075, 0.03)$. In [Figure 9](#), we compare LF + RK4 and LW + RK2 on 432×720 grid to a reference solution computed with LF + RK4 on a 4320×7200 grid. LW + RK2, computed with $\alpha = 3.6((\Delta x)^2 = (\Delta y)^2)$, preserves the fine details while the viscous regularization of LF + RK4 smoothes them out.

5.3.2. Shear shocks. We investigate the shear-like collision of two shock waves on $[0.0, 1.2] \times [0.0, 1.0]$, with periodic boundary conditions. We use initial conditions $u(x, y \leq 0.5, 0) \approx 2.5 \sin(2\pi(x-1)/1.2) + 1$, $u(x, y \geq 0.5, 0) \approx -1.5 \sin(2\pi(x-0.9)/1.2) - 1$, and $\rho(x, y, 0) \equiv 1$, ensuring a gradual transition at $y = 0$ and $y = 1$ using a smooth cutoff function. The layers $y \leq 0.5$ and $y \geq 0.5$ form shocks moving in opposite directions that collide in the shear layers causing interactions of shock waves with strong vortical flow. In [Figure 10](#), we compare LF + RK4 and LW + RK2 on 600×500 grid to a reference solution computed with LF + RK4 on a $1.2 \cdot 10^4 \times 10^4$ grid. LW + IGR + RK2, computed with $\alpha = 5((\Delta x)^2 = (\Delta y)^2)$, preserves the fine details while the viscous regularization of LF + RK4 smoothes them out. As shown in [Figure 11](#), LW + IGR + RK2 avoids the systematic loss of energy exhibited by LF + RK4. In [Figure 12](#) we show that LW + IGR + RK2 preserves sharp density gradients for much longer time horizons. In [Figure 13](#), we provide evidence that refining the mesh for constant α results in convergence to a well-defined solution of [\(4.1\)](#). Finally, in [Figure 14](#) we illustrate the convergence to the reference solution under decreasing α .

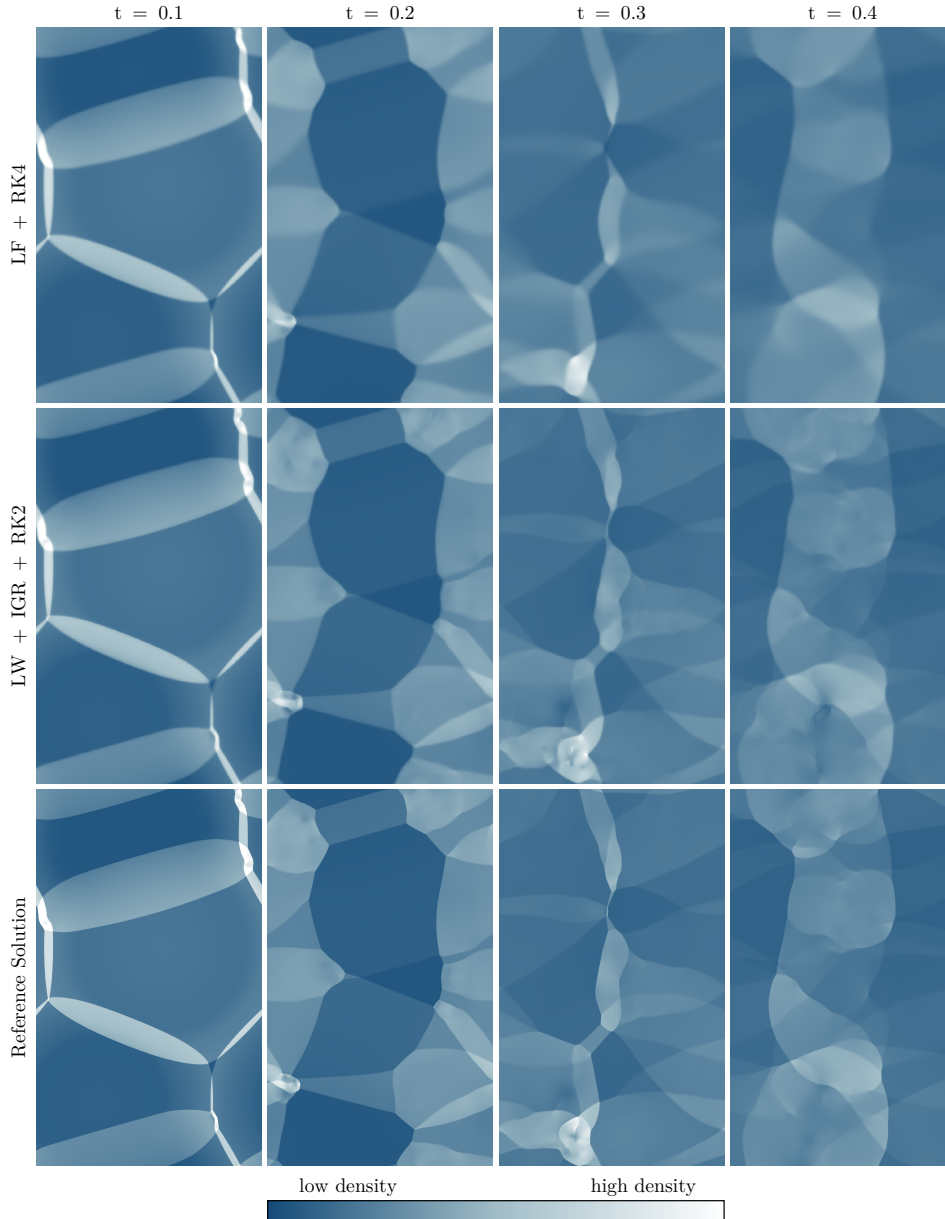


FIG. 9. *Blast waves.* We compare density plots of *Lax-Friedrichs* and *Lax-Wendroff with IGR* on a 432×720 grid to a reference solution computed by *Lax-Friedrichs* on a 4320×7200 grid.

6. Comparison, conclusion, and outlook.

6.1. Comparison to related work. The earliest work proposing inviscid regularization in a spirit similar to ours is a series of papers by Bhat and Fetecau [14, 13, 12], motivated by ideas of Leray [47]. In the case of Burgers' equation ($P \equiv 0$), their regularization amounts to setting $\rho \equiv 1$ in (3.5) and shows promising results. But its generalization to the Euler equation fails to maintain the shock

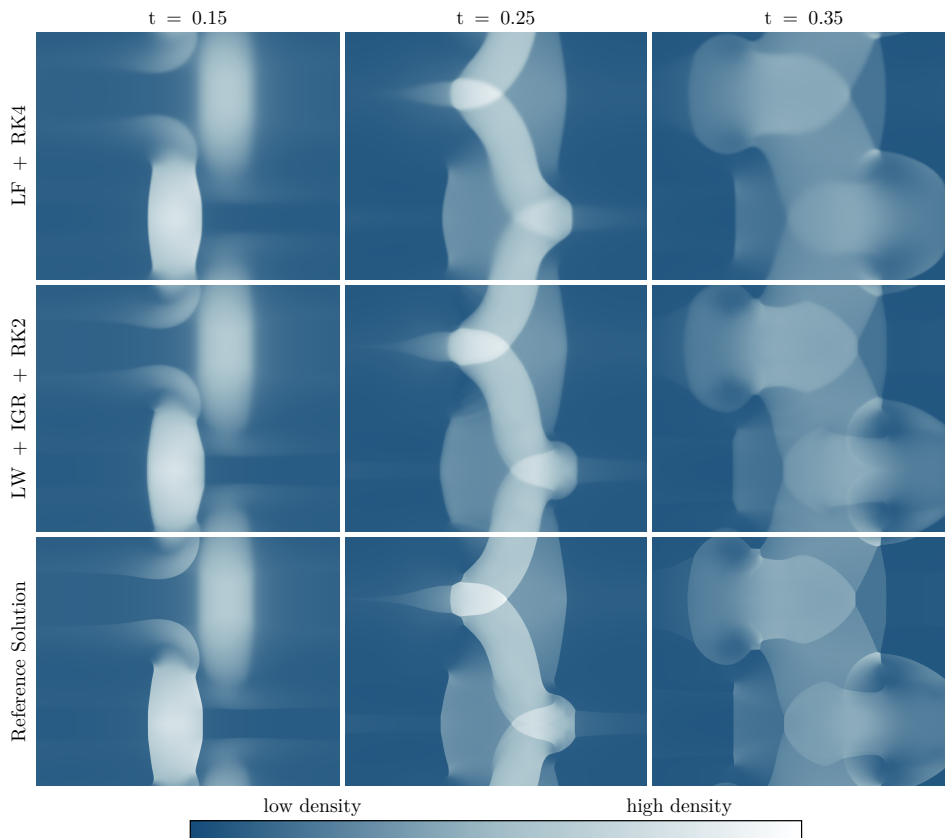


FIG. 10. *Shock collision.* We compare density plots of *Lax-Friedrichs* and *Lax-Wendroff* with *IGR* on a 600×500 grid to a reference solution computed by *Lax-Friedrichs* on a $1.2 \cdot 10^4 \times 10^4$ grid.

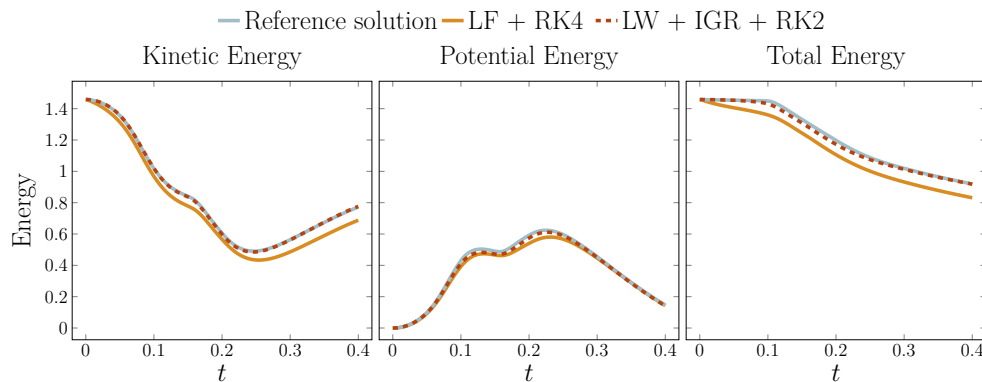


FIG. 11. *Nondissipative regularization.* We compare the energy dissipation of *Lax-Friedrichs* and *Lax-Wendroff* with *IGR* on a 600×500 grid to a reference solution computed by *Lax-Friedrichs* on a $10^4 \times 1.210^4$ grid. Contrary to *Lax-Friedrichs*'s, *IGR* solutions show no dissipative bias.

speed of the nominal equation, greatly limiting its usefulness for numerical purposes [12]. Recently, [37] proposed a family of inviscid and nondispersive regularizations for the unidimensional Euler equation, based on a similar regularization for the shal-

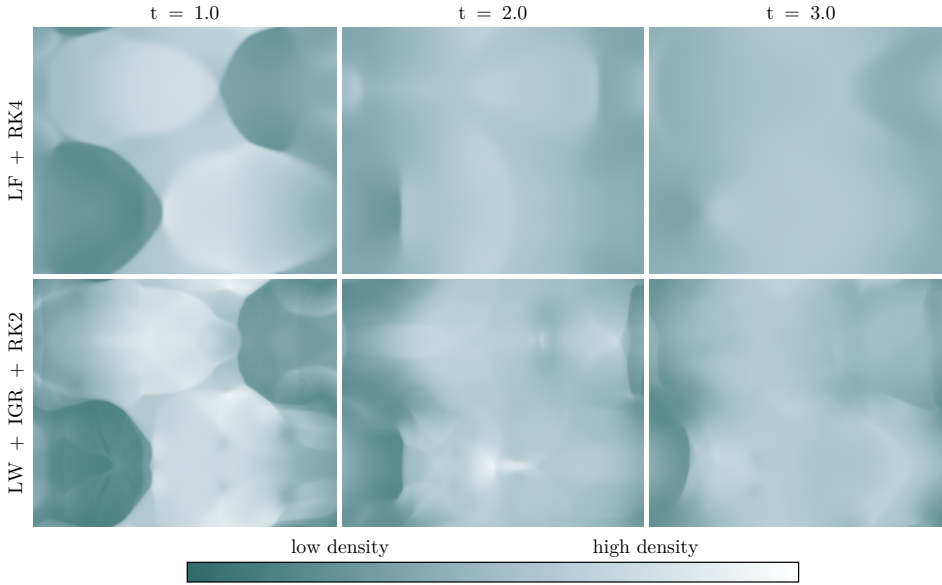


FIG. 12. **Preservation of density gradients.** When simulating the problem in *Figure 10* over a longer time horizon, the viscous regularization eventually loses the sharpness of the density gradients. In contrast, IGR maintains the steepness of density gradient.

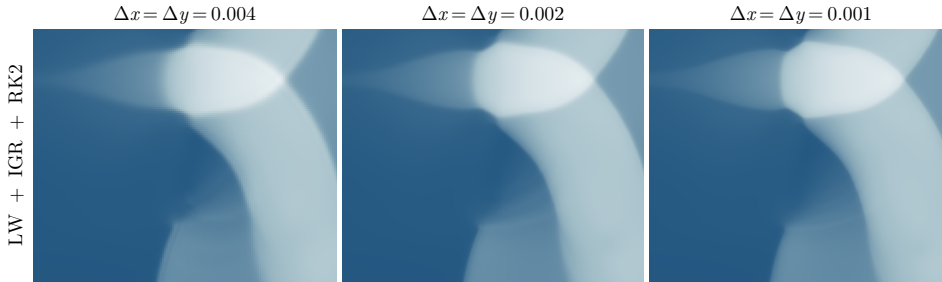


FIG. 13. **Mesh convergence.** As we increase the spatial resolution for constant $\alpha = 5 \cdot 10^{-5}$, the solutions appear to converge to a well-defined solution of the modified PDE.

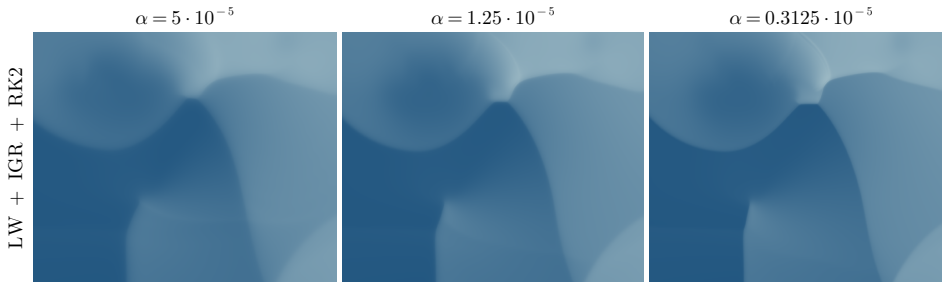


FIG. 14. As α decreases, the density gradients sharpen and the regularized solutions appear to converge to the nominal vanishing viscosity solution (plots with $\Delta x = \Delta y = 5 \cdot 10^{-4}$).

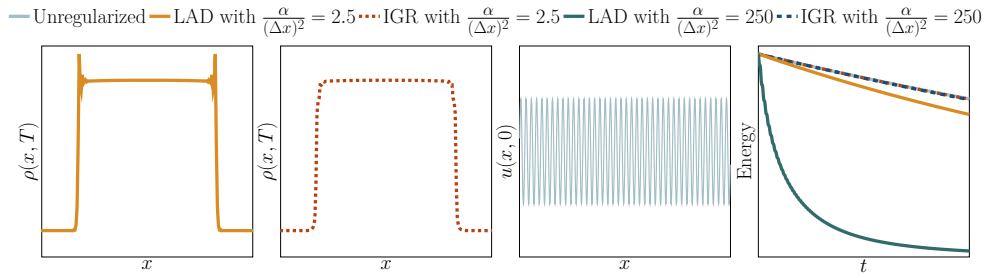


FIG. 15. **IGR versus localized artificial diffusivity (LAD).** The nonlocality of IGR reduces oscillations of dispersive schemes like Lax-Wendroff at shocks (first two panels). In high-frequency sound waves (third panel), LAD loses energy as each downward slope of u incurs dissipation. The antidissipation of IGR in upward slopes prevents this, even for 100 times larger α . (fourth panel)

low water equation [25]. The members of this family can be written in conservation form and thus maintain the correct shock speed. They are parametrized by a function $\mathcal{A} : \mathbb{R} \rightarrow \mathbb{R}$ of the density. In the special case of $P \equiv 0$ and $\mathcal{A}(\rho) := \rho$, this regularization coincides with (3.5). While [37] does not give this case special consideration and their proposed regularization is limited to the unidimensional case, their theoretical results may aid in understanding information geometric regularization. Numerous existing works apply viscous regularization adaptively, based on shock indicators [66, 57, 27, 32, 52, 10, 38, 17, 29, 11, 43]. In the unidimensional case, a prototypical form of this “localized artificial diffusivity” (LAD) amounts to removing the elliptic operator and using only the negative part of $[\partial_x u]$ in (3.5), yielding

$$\begin{cases} \partial_t \begin{pmatrix} \rho u \\ \rho \end{pmatrix} + \partial_x \begin{pmatrix} \rho u^2 + P(\rho) + \Sigma \\ \rho u \end{pmatrix} = \begin{pmatrix} f \\ 0 \end{pmatrix} \\ \rho^{-1} \Sigma - \alpha \partial_x (\rho^{-1} \partial_x \Sigma) = 2\alpha ([\partial_x u])_- [\partial_x u]. \end{cases}$$

Thus, the regularization term Σ of (3.5) mimics a nonlocal and sign-indefinite diffusion. As shown in Figure 15, the nonlocality due to the elliptic problem in IGR reduces spurious oscillations in dispersive numerical schemes for a given parameter α . Where LAD can impose limits on the time step sizes due to the quadratic scaling of parabolic CFL numbers [43], our experiments suggest that increasing α in IGR imposes no such restrictions, although it may increase the number of Jacobi or Gauss-Seidel sweeps per time steps needed to compute Σ . A striking difference between IGR and LAD is that the IGR “diffusion tensor” is sign-indefinite. As shown in Figure 15, this overcomes LAD’s systematic dissipative bias in high-frequency sound waves that otherwise requires specialized treatment [43]. In the multivariate case, IGR avoids energy dissipation due to shear motion, different from diffusive regularization. Similar considerations have motivated different variants of adaptive bulk viscosity (ABV) [27, 52] in the numerical solution of Navier Stokes problems. Indeed, the variant proposed by [52] (with parameter $r = 0, C = 2\alpha$) amounts to using $\Sigma = 2\alpha (\text{tr}(Du))_- (\text{tr}(Du))$ in IGR. But we find that without the $\text{tr}([Du]^2)$ term, both IGR and ABV are prone to vanishing density in strongly rotational flows. The Riemannian geometry induced by the squared L^2 -distance in the original Euler equation is closely related to the Wasserstein geometry on the space of mass densities [16, 46] and the logdet regularization equals the negative Shannon entropy of the mass density. Information geometric regularization compromises between them. Similarly, [42, 3, 4, 56, 49, 5, 19] combine optimal transport with entropic terms and information geometry and [44] use en-

tropic regularization to solve explicitly inequality-constrained PDEs. In providing a geometric approach to modeling the energy dissipation in a shock our work is also related to the geometric treatment of thermodynamic systems in [34, 35, 36, 67].

6.2. Conclusion. In this work, we have proposed an information geometric regularization of the barotropic compressible Euler equation and provided a proof of concept for its numerical application. To the best of our knowledge, this is the first work that regularizes continuum mechanical equations by modifying the geometry of the manifold of deformation maps. It thus opens up numerous directions for future work, including the application to other systems of PDEs, the use of different geometries, as well as the theoretical and numerical study of the resulting equations. For the sake of concreteness and conciseness, we have restricted this work to the case of the barotropic Euler equation and the information geometry induced by the logarithmic barrier. But generalizations to different geometries and equations like Navier Stokes and general Euler equations are straightforward to derive. An improved theoretical understanding of our approach will help identify its most promising applications.

6.3. Outlook: Toward information geometric mechanics. Our work combines the geometry governing the inertial movement of individual particles with the information geometry of distributions of particles. It thus takes the first step toward developing *information geometric mechanics* that accounts for the geometries not just of fundamental physical laws governing describing microscopic behavior, but also of the statistical summaries describing their emergent macroscopic behavior.

Acknowledgments. The authors gratefully acknowledge support from the Air Force Office of Scientific Research under award number FA9550-23-1-0668 (Information Geometric Regularization for Simulation and Optimization of Supersonic Flow). RC acknowledges support through a PURA travel award from the Georgia Tech Office of Undergraduate Education.

REFERENCES

- [1] S.-I. AMARI, *Information geometry and its applications*, vol. 194, Springer, 2016.
- [2] S.-I. AMARI AND A. CICHOCKI, *Information geometry of divergence functions*, Bulletin of the polish academy of sciences. Technical sciences, 58 (2010), pp. 183–195.
- [3] S.-I. AMARI, R. KARAKIDA, AND M. OIZUMI, *Information geometry connecting Wasserstein distance and Kullback–Leibler divergence via the entropy-relaxed transportation problem*, Information Geometry, 1 (2018), pp. 13–37.
- [4] S.-I. AMARI, R. KARAKIDA, M. OIZUMI, AND M. CUTURI, *Information geometry for regularized optimal transport and barycenters of patterns*, Neural computation, 31 (2019), pp. 827–848.
- [5] S.-I. AMARI AND T. MATSUDA, *Information geometry of Wasserstein statistics on shapes and affine deformations*, arXiv preprint arXiv:2307.12508, (2023).
- [6] S.-I. AMARI AND H. NAGAOKA, *Methods of information geometry*, vol. 191, American Mathematical Soc., 2000.
- [7] V. ARNOLD, *Sur la géométrie différentielle des groupes de lie de dimension infinie et ses applications à l’hydrodynamique des fluides parfaits*, in Annales de l’institut Fourier, vol. 16, 1966, pp. 319–361.
- [8] N. AY, J. JOST, H. VÂN LÊ, AND L. SCHWACHHÖFER, *Information geometry*, vol. 64, Springer, 2017.
- [9] J. M. BALL, *Convexity conditions and existence theorems in nonlinear elasticity*, Archive for rational mechanics and Analysis, 63 (1976), pp. 337–403.
- [10] G. E. BARTER AND D. L. DARMOFAL, *Shock capturing with PDE-based artificial viscosity for DGFEM: Part I. formulation*, Journal of Computational Physics, 229 (2010), pp. 1810–1827.
- [11] A. BHAGATWALA AND S. K. LELE, *A modified artificial viscosity approach for compressible turbulence simulations*, Journal of computational physics, 228 (2009), pp. 4965–4969.

- [12] H. BHAT AND R. FETECAU, *On a regularization of the compressible Euler equations for an isothermal gas*, Journal of mathematical analysis and applications, 358 (2009), pp. 168–181.
- [13] H. BHAT AND R. FETECAU, *The Riemann problem for the Leray–Burgers equation*, Journal of Differential Equations, 246 (2009), pp. 3957–3979.
- [14] H. S. BHAT AND R. C. FETECAU, *A Hamiltonian regularization of the Burgers equation*, Journal of Nonlinear Science, 16 (2006), pp. 615–638.
- [15] D. BODONY AND A. FIKL, *Adjoint-based sensitivity of shock-laden flows*, (2022).
- [16] Y. BRENIER, *The least action principle and the related concept of generalized flows for incompressible perfect fluids*, Journal of the American Mathematical Society, 2 (1989), pp. 225–255.
- [17] O. P. BRUNO, J. S. HESTHAVEN, AND D. V. LEIBOVICI, *FC-based shock-dynamics solver with neural-network localized artificial-viscosity assignment*, Journal of Computational Physics: X, 15 (2022), p. 100110.
- [18] S. BUBECK, *Convex optimization: Algorithms and complexity*, Foundations and Trends in Machine Learning, 8 (2015), pp. 231–357.
- [19] M. BURGER, M. ERBAR, F. HOFFMANN, D. MATTHES, AND A. SCHLICHTING, *Covariance-modulated optimal transport and gradient flows*, arXiv preprint arXiv:2302.07773, (2023).
- [20] N. N. CHENTSOV, *Statistical decision rules and optimal inference*, no. 53, American Mathematical Soc., 2000.
- [21] D. CHRISTODOULOU, *The formation of shocks in 3-dimensional fluids*, vol. 2, European Mathematical Society, 2007.
- [22] D. CHRISTODOULOU, *The shock development problem*, 2019.
- [23] D. CHRISTODOULOU AND S. KLAINERMAN, *The global nonlinear stability of the Minkowski space*, Séminaire Équations aux dérivées partielles (Polytechnique) dit aussi” Séminaire Goulaouic-Schwartz”, (1993), pp. 1–29.
- [24] D. CHRISTODOULOU AND S. MIAO, *Compressible flow and Euler’s equations*, vol. 9, International Press Somerville, MA, 2014.
- [25] D. CLAMOND AND D. DUTYKH, *Non-dispersive conservative regularisation of nonlinear shallow water (and isentropic Euler equations)*, Communications in Nonlinear Science and Numerical Simulation, 55 (2018), pp. 237–247.
- [26] B. D. COLEMAN AND W. NOLL, *On the thermostatics of continuous media*, Archive for rational mechanics and analysis, 4 (1959), pp. 97–128.
- [27] A. W. COOK AND W. H. CABOT, *Hyperviscosity for shock-turbulence interactions*, Journal of Computational Physics, 203 (2005), pp. 379–385.
- [28] B. DACOROGNA, *Direct methods in the calculus of variations*, vol. 78, Springer Science & Business Media, 2007.
- [29] V. DOLEŽAL, M. FEISTAUER, AND C. SCHWAB, *On some aspects of the discontinuous Galerkin finite element method for conservation laws*, Mathematics and Computers in Simulation, 61 (2003), pp. 333–346.
- [30] D. G. EBIN AND J. MARSDEN, *Groups of diffeomorphisms and the motion of an incompressible fluid*, Annals of Mathematics, (1970), pp. 102–163.
- [31] L. C. EVANS, *Partial differential equations*, vol. 19, American Mathematical Society, 2022.
- [32] B. FIORINA AND S. K. LELE, *An artificial nonlinear diffusivity method for supersonic reacting flows with shocks*, Journal of Computational Physics, 222 (2007), pp. 246–264.
- [33] A. FUJIWARA, *Hommage to Chentsov’s theorem*, Information Geometry, (2022), pp. 1–20.
- [34] F. GAY-BALMAZ AND H. YOSHIMURA, *A Lagrangian variational formulation for nonequilibrium thermodynamics. part i: discrete systems*, Journal of Geometry and Physics, 111 (2017), pp. 169–193.
- [35] F. GAY-BALMAZ AND H. YOSHIMURA, *A Lagrangian variational formulation for nonequilibrium thermodynamics. part ii: continuum systems*, Journal of Geometry and Physics, 111 (2017), pp. 194–212.
- [36] F. GAY-BALMAZ AND H. YOSHIMURA, *From Lagrangian mechanics to nonequilibrium thermodynamics: a variational perspective*, Entropy, 21 (2018), p. 8.
- [37] B. GUELMAME, D. CLAMOND, AND S. JUNCA, *Hamiltonian regularisation of the unidimensional barotropic Euler equations*, Nonlinear Analysis: Real World Applications, 64 (2022), p. 103455.
- [38] J.-L. GUERMOND, R. PASQUETTI, AND B. POPOV, *Entropy viscosity method for nonlinear conservation laws*, Journal of Computational Physics, 230 (2011), pp. 4248–4267.
- [39] J.-L. GUERMOND AND B. POPOV, *Viscous regularization of the Euler equations and entropy principles*, SIAM Journal on Applied Mathematics, 74 (2014), pp. 284–305.
- [40] O. GÜLER, *Barrier functions in interior point methods*, Mathematics of Operations Research,

- 21 (1996), pp. 860–885.
- [41] A. HARTEN, B. ENQUIST, S. OSHER, AND S. R. CHAKRAVARTHY, *Uniformly high order accurate essentially non-oscillatory schemes, III*, Journal of computational physics, 131 (1997), pp. 3–47.
- [42] R. JORDAN, D. KINDERLEHRER, AND F. OTTO, *The variational formulation of the Fokker–Planck equation*, SIAM journal on mathematical analysis, 29 (1998), pp. 1–17.
- [43] S. KAWAI, S. K. SHANKAR, AND S. K. LELE, *Assessment of localized artificial diffusivity scheme for large-eddy simulation of compressible turbulent flows*, Journal of computational physics, 229 (2010), pp. 1739–1762.
- [44] B. KEITH AND T. M. SUROWIEC, *Proximal Galerkin: A structure-preserving finite element method for pointwise bound constraints*, arXiv preprint arXiv:2307.12444, (2023).
- [45] B. KHESIN AND G. MISIOLEK, *Shock waves for the Burgers equation and curvatures of diffeomorphism groups*, Proceedings of the Steklov Institute of Mathematics, 259 (2007), p. 73.
- [46] B. KHESIN, G. MISIOLEK, AND K. MODIN, *Geometric hydrodynamics and infinite-dimensional newton’s equations*, Bulletin of the American Mathematical Society, 58 (2021), pp. 377–442.
- [47] J. LERAY, *Essai sur le mouvement d’un fluide visqueux emplissant l’espace*, Acta Math., 63 (1934), pp. 193–248.
- [48] R. J. LEVEQUE AND R. J. LEVEQUE, *Numerical methods for conservation laws*, vol. 214, Springer, 1992.
- [49] W. LI AND J. ZHAO, *Wasserstein information matrix*, Information Geometry, (2023), pp. 1–53.
- [50] X.-D. LIU, S. OSHER, AND T. CHAN, *Weighted essentially non-oscillatory schemes*, Journal of computational physics, 115 (1994), pp. 200–212.
- [51] C. LOZANO, *Watch your adjoints! Lack of mesh convergence in inviscid adjoint solutions*, AIAA Journal, 57 (2019), pp. 3991–4006.
- [52] A. MANI, J. LARSSON, AND P. MOIN, *Suitability of artificial bulk viscosity for large-eddy simulation of turbulent flows with shocks*, Journal of Computational Physics, 228 (2009), pp. 7368–7374.
- [53] A. S. NEMIROVSKI AND M. J. TODD, *Interior-point methods for optimization*, Acta Numerica, 17 (2008), pp. 191–234.
- [54] A. S. NEMIROVSKIJ AND D. B. YUDIN, *Problem complexity and method efficiency in optimization*, (1983).
- [55] Y. E. NESTEROV, M. J. TODD, ET AL., *On the Riemannian geometry defined by self-concordant barriers and interior-point methods*, Foundations of Computational Mathematics, 2 (2002), pp. 333–361.
- [56] G. PEYRÉ, M. CUTURI, ET AL., *Computational optimal transport: With applications to data science*, Foundations and Trends® in Machine Learning, 11 (2019), pp. 355–607.
- [57] G. PUPPO, *Numerical entropy production for central schemes*, SIAM Journal on Scientific Computing, 25 (2004), pp. 1382–1415.
- [58] G. RASKUTTI AND S. MUKHERJEE, *The information geometry of mirror descent*, IEEE Transactions on Information Theory, 61 (2015), pp. 1451–1457.
- [59] D. RAY AND J. S. HESTHAVEN, *An artificial neural network as a troubled-cell indicator*, Journal of computational physics, 367 (2018), pp. 166–191.
- [60] Y. SAAD, *Iterative methods for sparse linear systems*, SIAM, 2003.
- [61] F. SCHÄFER, A. ANANDKUMAR, AND H. OWHADI, *Competitive mirror descent*, arXiv preprint arXiv:2006.10179, (2020).
- [62] A. SCHMEDING, *An Introduction to Infinite-Dimensional Differential Geometry*, Cambridge Studies in Advanced Mathematics, Cambridge University Press, 2022, <https://doi.org/10.1017/9781009091251>.
- [63] C.-W. SHU, *Advanced numerical approximation of nonlinear hyperbolic equations, chapter essentially non-oscillatory and weighted essentially non-oscillatory schemes for hyperbolic conservation laws*, 1998.
- [64] T. C. SIDERIS, *Formation of singularities in three-dimensional compressible fluids*, Communications in mathematical physics, 101 (1985), pp. 475–485.
- [65] B. VAN LEER, *Towards the ultimate conservative difference scheme. V. a second-order sequel to Godunov’s method*, Journal of computational Physics, 32 (1979), pp. 101–136.
- [66] J. VONNEUMANN AND R. D. RICHTMYER, *A method for the numerical calculation of hydrodynamic shocks*, Journal of applied physics, 21 (1950), pp. 232–237.
- [67] H. YOSHIMURA AND F. GAY-BALMAZ, *Hamiltonian variational formulation for non-simple thermodynamic systems*, in International Conference on Geometric Science of Information, Springer, 2023, pp. 221–230.